

# Acoustic Receptivity of Compressible Boundary Layers: Receptivity via Surface-Temperature Variations

---

*Meelan Choudhari*  
*High Technology Corporation • Hampton, Virginia*



# Acoustic Receptivity of Compressible Boundary Layers: Receptivity via Surface-Temperature Variations

Meelan Choudhari  
High Technology Corporation  
Hampton, VA 23666

## Abstract

The Goldstein-Ruban theory has been extended within the quasi-parallel framework of Zavol'skii *et al.* to study the acoustic receptivity of compressible boundary layers. We consider the receptivity produced in a region of localized, small-amplitude variation in the surface temperature and compare it with the receptivity that is induced through a similar mechanism by a variation in the suction velocity at the surface. The orientation of the acoustic wave can have a significant impact on the receptivity process, with the maximum receptivity at a given sound-pressure level produced by upstream-oriented acoustic waves. At sufficiently low Mach numbers, the variation of receptivity with the acoustic-wave orientation can be predicted analytically and is the same for both surface suction and surface heating. However, as a result of the acoustic refraction across the mean boundary layer, the above dependence can become complex and dependent upon the type of surface nonuniformity. The results also suggest that the receptivity caused by temperature nonuniformities may turn out to be more significant than that produced by the mean-flow perturbations associated with strip suction.

## 1. Introduction

The central issue in regard to the generation of instability waves in low-speed boundary layers was the identification of the wavelength-reduction mechanisms that enable the long-wavelength free-stream disturbances to excite short-wavelength instability waves (Reshotko 1976, Goldstein 1983). The pioneering work of Goldstein (1983, 1985), as well as that of Zavol'skii *et al.* (1983), Ruban (1985), and Goldstein *et al.* (1987), showed that the key to this wavelength-reduction process is the occurrence of sufficiently shorter length scales in the mean flow, which can tune the free-stream disturbance to the length

scale of the boundary-layer eigensolutions. These short-scale variations may occur either naturally (because of the rapid development of a boundary-layer flow in the vicinity of the leading edge (Goldstein 1983)), or may be induced externally (by a short-scale variation in the surface boundary conditions). Examples in the second category include irregularities in the shape of the airfoil surface (Zavol'skii *et al.* 1983, Goldstein 1985, Ruban 1985) and nonuniformities in the surface distributions of suction velocity and surface admittance (Kerschen and Choudhari 1985). The theories of Goldstein, Zavol'skii *et al.*, and Ruban have subsequently been applied to a variety of problems, and the reader is referred to the reviews by Goldstein and Hultgren (1989) and Kerschen (1989), as well as to the relevant papers in Reda *et al.* (1991). Many significant contributions in the area of boundary-layer receptivity have been reported in the Russian literature as well, and some of those papers have been reviewed by Nishioka and Morkovin (1986) and Kozlov and Ryzhov (1990).

Much of the above research was related to the acoustic generation of instability waves and focused on the incompressible flow regime, in which the wavelength of acoustic disturbances is effectively infinite. The acoustic wavelength shortens progressively (in comparison with the convective length scale at the same frequency) as the Mach number is increased. However, it remains asymptotically larger than the wavelength of the viscous-inviscid interactive Tollmien-Schlichting mode (TS) (Ryzhov and Zhuk 1986, Smith 1989) which dominates the primary instability of two-dimensional boundary layers at subsonic and moderately supersonic speeds. Consequently, the wavelength reduction mechanisms previously identified by Goldstein (1983, 1985), and Ruban (1985) are also directly relevant to the generation of the viscous-inviscid interactive modes in compressible boundary layers.

At high supersonic and hypersonic Mach numbers, the dominant instabilities of a boundary-layer flow are predominantly inviscid, and their phase speeds (or wavelengths) are comparable to those of the acoustic disturbances in the free stream. However, because these inviscid instabilities (i.e., Rayleigh modes) are primarily subsonic with respect to the local free stream, their phase speeds do not match with the acoustic propagation speed (except in a limiting sense as described in the following paragraph). Therefore, a spatial tuning of the unsteady motion (forced by the free-stream disturbances) is still necessary for the excitation of the inviscid instabilities. This tuning can be provided by the short-scale surface nonuniformities in much the same manner as that in the incompressible boundary layers. However, the asymptotic scaling involved is completely different for the inviscid modes of supersonic boundary layers. Accordingly, the details of the energy transfer process can be significantly different in the two speed regimes, as discussed by Choudhari and Streett (1990). This work describes the extension of the Goldstein-Ruban theory to high-speed boundary layers and presents numerical results for both viscous-inviscid interactive modes and predominantly inviscid Rayleigh instabilities. However, because the main purpose of that paper was to provide an overview of the receptivity of high-speed boundary layers, only a few sets of results were presented.

The limiting case mentioned in the preceding paragraph involves a resonance in the leading-edge region of a flat-plate boundary layer between the inviscid instability modes and the acoustic free-stream disturbances that propagate parallel to the plate (Gaponov 1985). The strong excitation of instability waves by such "grazing" acoustic disturbances was recently explained by Fedorov and Khokhlov (1991) with a theory that is the supersonic analog of Goldstein's (1983) seminal work on TS-mode generation near the leading edge of a flat-plate airfoil. Because of the above-mentioned resonance feature, the study of leading-edge receptivity in a highly supersonic boundary layer reduces to a study of the sound-generation mechanisms that excite the grazing acoustic disturbance via a scattering process near the leading edge. (See the more recent work of Fedorov and Khokhlov (1993) in this context.)

In addition to the receptivity produced near the leading edge and the receptivity caused by scattering near surface nonuniformities, other possible mechanisms ex-

ist through which a TS or a Rayleigh instability can be excited in a supersonic boundary layer. These mechanisms include a resonant forcing through the quadratic interaction between a pair of acoustic and convected free-stream disturbances, and a sustained generation of three-dimensional TS waves through the interaction of slow, near-planar acoustic disturbances and long-wavelength Görtler vortices. However, these mechanisms are somewhat specialized, and one may expect the overall receptivity to be dominated by the leading-edge mechanism and the surface nonuniformities. The relative importance of the two dominant routes for receptivity will depend crucially upon the Mach number of the flow, as well as on the leading-edge geometry and the amplitude and spatial distribution of the surface nonuniformities. This particular issue is beyond the scope of this paper and, therefore, will be addressed in a future article.

In this paper, we will examine in further detail the generation of viscous and inviscid instabilities via the interaction of a time-harmonic acoustic disturbance with short-scale small-amplitude variations in the surface distributions of suction velocity and temperature. The effectiveness of strip suction and strip heating in stabilizing gas boundary layers at subsonic speeds was demonstrated theoretically by Reed and Nayfeh (1985) and Masad and Nayfeh (1992), respectively. However, the mean-flow disturbance induced by these devices can also act as a catalyst in the receptivity process, as described above. The receptivity due to both localized and nonlocalized variations in the suction-velocity distribution was studied in the context of low-speed flows by Kerschen and Choudhari (1985) and Choudhari (1992), respectively; Choudhari and Streett (1990) investigated the localized receptivity in high-speed flows. The use of surface heating or cooling for laminar flow control (LFC) is primarily relevant to the case of high-speed boundary layers, and the associated receptivity mechanism does not appear to have been studied thus far.

As shown by Kerschen and Choudhari (1985), two distinct scattering mechanisms are responsible for the acoustic receptivity induced by a porous surface that is typically used for suction-based LFC. These two mechanisms are (1) scattering by the short-scale mean-flow variations produced by a specified surface-suction distribution and (2) scattering by variations in the acoustic admittance of the porous surface. When the amplitudes of both variations are sufficiently small, the receptivity

produced via each mechanism can be examined independently of the other mechanism. In this paper, we focus on the receptivity produced in the zero-admittance limit (i.e., on the receptivity that occurs through the mean-flow variations only). A comparison will be made with the analogous receptivity mechanism in the case of heat-transfer strips at the surface. Receptivity that occurs via surface admittance variations is studied in a separate paper, wherein we also examine the effect of a nonzero surface admittance on the stability of a compressible boundary layer.

Generally, in this paper we focus on the localized receptivity process associated with a single suction, heating, or cooling strip. However, receptivity produced in noncompact LFC configurations that involve a series of such strips will also be considered briefly. To predict the outcome of the localized receptivity process, we utilize a nonasymptotic extension of the Goldstein-Ruban theory, which was summarized by Choudhari and Streett (1990). A similar approach was used earlier by Choudhari and Streett (1991) to predict the suction-induced receptivity in low-speed boundary layers. The assumption of a small-amplitude surface disturbance may appear to be somewhat restrictive in terms of applying the theory in practice. However, this assumption simplifies the analysis to a great extent; moreover, it enables fairly general conclusions to be drawn in regard to the receptivity produced by different possible combinations of free-stream and surface disturbances, irrespective of the particular geometry involved. (See Goldstein 1985.) A brief description of the above nonasymptotic approach applied to compressible boundary layers is given in section 2 below. The numerical results, which are obtained for a flat-plate boundary layer at various Mach numbers, are presented in section 3. Conclusions are given in section 4.

## 2. Description of the Analysis Involved

Consider the uniform two-dimensional steady supersonic flow of a perfect gas past an infinitely thin and nominally flat airfoil that has a localized nonuniformity in the surface distributions of suction velocity and/or the temperature at a distance  $\ell^*$  from the leading edge. The velocity of the oncoming free stream is denoted by  $U_\infty^*$ , and the corresponding Mach number is symbolized by  $M$ . The pressure, temperature, density, absolute viscosity, and specific heat at constant pressure at the free-stream conditions are denoted by  $P_\infty^*$ ,  $T_\infty^*$ ,  $\rho_\infty^*$ ,  $\mu_\infty^*$ , and

$C_{p,\infty}^*$ , respectively; the ratio of the specific heat at constant pressure to that at constant volume is denoted by  $\gamma$ . We now assume that the local distributions of the surface suction velocity and the surface temperature are given by

$$V_w^*/U_\infty^* = \epsilon_w^{(s)} F_w^{(s)}(X, Z), \quad (1a)$$

and

$$T_w^*/T_\infty^* = T_{w,0} + \epsilon_w^{(t)} F_w^{(t)}(X, Z), \quad (1b)$$

respectively. The amplitude parameters  $\epsilon_w^{(s)}$  and  $\epsilon_w^{(t)}$  are assumed to be sufficiently small, so that the mean-flow disturbance produced by each type of nonuniformity can be treated as a small perturbation to the unperturbed mean boundary layer. The quantity  $T_{w,0}$  in (1b) represents the local (nondimensional) surface temperature for the unperturbed mean flow. The nondimensional functions  $F_w^{(s)}(X, Z)$  and  $F_w^{(t)}(X, Z)$  denote the normalized distributions of suction velocity and surface temperature in terms of the local coordinates

$$X \equiv (x^* - \ell^*)/\delta^* \text{ and } Z \equiv z^*/\delta^* \quad (1c)$$

along the streamwise and spanwise directions, respectively, where  $\delta^*$  is the local displacement thickness associated with the unperturbed mean boundary layer.

The unsteady free-stream disturbance incident upon the surface irregularity is assumed to be a time-harmonic acoustic wave with the frequency  $\omega^*$  (comparable to the range of locally unstable frequencies), the streamwise wavenumber  $\alpha_{ac}^*$ , and the spanwise wavenumber  $\beta_{ac}^*$ . We use the symbol  $\epsilon_{ac}$  to denote the nondimensional amplitude of this wave, which is assumed to have been defined in terms of the amplitude of the acoustic fluctuation in an appropriate flow variable and normalized by a suitable quantity associated with the mean flow. For now, we will leave open the choice of the flow quantities involved in defining  $\epsilon_{ac}$  and will simply assume that the latter parameter is sufficiently small, so that the unsteady part of the motion can always be treated as a small perturbation to the local mean flow throughout the region of interest.

As first shown by Goldstein (1985) and Ruban (1985), the problem of studying the interaction of the acoustic wave with the steady nonuniformity on the airfoil surface is simplified considerably after the small-disturbance approximation ( $\epsilon_w^{(s)}, \epsilon_w^{(t)} \ll 1$ ,  $\epsilon_{ac} \ll 1$ ) is invoked and the local nature of the interaction process ( $\delta^* \ll \ell^*$ ) is exploited. Specifically, if we use

$U_\infty^*$ ,  $\rho_\infty^* U_\infty^{*2}$ , and  $T_\infty^*$  to nondimensionalize the local velocities, pressure, and temperature, respectively, and denote the corresponding nondimensional quantities by dropping the superscript  $*$  on them, then we can expand the array of dependent variables  $\mathbf{Q} = (U, V, W, T, P)$  for each type of surface nonuniformity in terms of the two-parameter perturbation series

$$\begin{aligned} \mathbf{Q}^{(j)}(X, Y, Z, t) = & \mathbf{Q}_0(Y) + \epsilon_w^{(j)} \mathbf{Q}_w^{(j)}(X, Y, Z) \\ & + \epsilon_{ac} \mathbf{Q}_{ac}(Y) e^{i[\alpha_{ac} X + \beta_{ac} Z - \omega t]} \\ & + \epsilon_w^{(j)} \epsilon_{ac} \mathbf{Q}_{w,ac}^{(j)}(X, Y, Z) e^{-i\omega t} \\ & + O(\epsilon_w^{(j)2}, \epsilon_{ac}^2), \end{aligned} \quad (2a)$$

where the superscript  $j$  indicates whether the surface nonuniformity involves a short-scale variation in the suction velocity ( $j = s$ ) or in the surface temperature ( $j = t$ ). The wall-normal coordinate  $Y$  has been scaled with respect to  $\delta^*$ , whereas the frequency  $\omega$  and time  $t$  have been normalized by  $U_\infty^*/\delta^*$  and its inverse, respectively. Implicit in the form of (2a) is the assumption that the unperturbed boundary-layer flow is convectively unstable (Huerre and Monkewitz, 1990) at the location of interest. This assumption is central to most problems of receptivity, as discussed by Goldstein (1985).

The nonzero elements of the zeroth-order term

$$\mathbf{Q}_0(Y) = (U_0(Y), 0, 0, T_0(Y), \frac{1}{\gamma M_\infty^2}) \quad (2b)$$

denote the quasi-parallel approximations to the corresponding base-flow quantities at  $x^* = \ell^*$ . The first-order perturbations due to the wall nonuniformity and the free-stream acoustic wave are indicated by the subscripts  $w$  and  $ac$ , respectively. We can easily show that the mean-flow disturbance  $\mathbf{Q}_w^{(j)}$  due to the surface nonuniformity satisfies the steady version of the parallel-flow disturbance equations (Lekoudis *et al.* 1976), subject to inhomogeneous boundary conditions at the surface that are appropriate for the type of nonuniformity involved. It is necessary to point out that the surface-temperature variation induces a change in the local mean flow through changes in both the density and the viscosity of the flow. In this paper, we will not make any attempt to assess the separate contributions to the mean-flow perturbation through the above two channels; however, we expect that for  $M = O(1)$  the dominant contribution will be provided by the changes in the density of the flow. The signature

$\mathbf{Q}_{ac}$  of the acoustic disturbance within the mean boundary layer satisfies the unsteady parallel-flow disturbance equations, subject to outer boundary conditions appropriate for the specified form of the incoming disturbance (Mack 1984).

Neither of the two first-order perturbations simultaneously possesses the combination of length and time scales relevant to the local instability motion. However, this required combination is produced by the scattering of the acoustic-signature field by the mean-flow disturbance. The leading-order solution for this scattered field is given by the  $O(\epsilon_w^{(j)} \epsilon_{ac})$  term in (2a) (i.e., the term that contains  $\mathbf{Q}_{w,ac}^{(j)}$ ), which represents the bilinear interaction between the first-order perturbations  $\mathbf{Q}_w^{(j)}$  and  $\mathbf{Q}_{ac}$ . After a Fourier transform is taken along the streamwise ( $X \rightarrow \alpha$ ) and spanwise ( $Z \rightarrow \beta$ ) directions,  $\mathbf{Q}_{w,ac}^{(j)}$  satisfies an inhomogeneous form of the linear stability equations

$$\mathbf{L}_{NS}(\alpha, \partial_Y, \beta, \omega, R_{\delta^*}) \bar{\mathbf{Q}}_{w,ac}^{(j)} = \mathbf{N}_{NS;2}(\bar{\mathbf{Q}}_w^{(j)}, \mathbf{Q}_{ac}), \quad (3)$$

in which the overbar denotes the Fourier transformed quantities.

The operator  $\mathbf{L}_{NS}$  on the left-hand side of (3) denotes the matrix form of the linearized continuity and Navier-Stokes equations in the transform space  $(\alpha, \beta)$ , and  $R_{\delta^*} \equiv \rho_\infty^* U_\infty^* \delta^* / \mu_\infty^*$  is the Reynolds number based on the local displacement thickness of the unperturbed boundary layer. The expression for  $\mathbf{L}_{NS}$  can be found in different equivalent forms in the literature on the quasi-parallel stability of compressible shear flows. The forcing vector  $\mathbf{N}_{NS;2}$  on the right-hand side represents the bilinear interaction (indicated by the subscript 2) between its vector arguments  $\bar{\mathbf{Q}}_w^{(j)}$  and  $\mathbf{Q}_{ac}$ . It arises from the convective and viscous nonlinearities in the exact governing equations. The expressions for the elements of  $\mathbf{N}_{NS;2}$  are provided in the appendix. Even though we are interested only in the receptivity of a two-dimensional base flow in this paper, the expressions given in the appendix are general and may be applied to arbitrary three-dimensional base flows and other types of free-stream disturbances. In fact, with a suitable modification of the terms that involve  $\omega$ , the same expressions may be utilized in a study of resonant triad interactions among disturbances in compressible shear flows. As pointed out by Choudhari and Streett (1990), similar interactions that involve an appropriate combination of an acoustic and a convected free-stream disturbance could also lead to receptivity in

high-speed boundary layers. However, the receptivity via this latter mechanism is expected to be relatively weak in view of the quadratic dependence of receptivity on the amplitude level of the free-stream disturbances, which is typically very small.

Depending on the geometry  $F^{(j)}(X, Z)$  of a three-dimensional surface nonuniformity, the instability motion excited in its vicinity can have a considerably complex spatial structure. However, because the interaction that leads to this receptivity process is bilinear, the instability waves that are produced via each spanwise Fourier component of  $F^{(j)}(X, Z)$  can be analyzed independently. Therefore, we will confine our attention for the remainder of this work to those surface disturbances that are periodic in the  $Z$  direction with a (single) wave number  $\beta = \beta_w$ . That is, we will focus on cases where

$$F^{(j)}(X, Z) = \mathcal{F}^{(j)}(X) e^{i\beta_w Z}. \quad (4a)$$

The numerical results to be presented in section 3 correspond exclusively to two-dimensional surface disturbances (i.e., to the special case  $\beta_w = 0$ ). In view of (4a), the unsteady scattered field  $\mathbf{Q}_{w,ac}^{(j)}$  has the form

$$\mathbf{Q}_{w,ac}^{(j)}(X, Y, Z) = \mathbf{Q}_{w,ac}^{(j)}(X, Y) e^{i(\beta_{ac} + \beta_w)Z}. \quad (4b)$$

The part of  $\mathbf{Q}_{w,ac}^{(j)}$  that corresponds to the instability mode of interest can be found as the residue contribution to the inverse Fourier integral

$$\mathbf{Q}_{w,ac}^{(j)}(X, Y) = \frac{1}{\sqrt{2\pi}} \int_{-\infty}^{\infty} \bar{\mathbf{Q}}_{w,ac}^{(j)}(\alpha, Y) e^{i\alpha Z} d\alpha \quad (5a)$$

from an appropriate singularity of the transform solution  $\bar{\mathbf{Q}}_{w,ac}^{(j)}(\alpha, Y)$  in the streamwise wave-number ( $\alpha$ ) space (Goldstein 1985, Ruban 1985). In general, this singularity assumes the form of a first-order pole, and its location is given by the spatial dispersion relation

$$\alpha = \alpha_{ins}(\beta_{ins}, \omega, R_{\delta^*}) \quad (\beta_{ins} \equiv \beta_{ac} + \beta_w) \quad (5b)$$

for the instability mode under consideration. As a result of isolating the instability-wave part of the unsteady scattered field, one is able to relate the amplitude of the generated wave to the amplitude of the incident acoustic wave. Thus, the dimensional perturbation in the streamwise component of the unsteady mass flux that is associated with the generated instability wave can be expressed in the form (Goldstein 1985, Choudhari and Streett 1990)

$$(\rho U)_{ins}^*(X, Y, Z, t) =$$

$$(\rho U)_{ac,i}^* C_{\rho U; \rho U}^{(j)} E_{\rho U}(Y) e^{i[\alpha_{ins} X + (\beta_w + \beta_{ac})Z - \omega t]}, \quad (6a)$$

where  $\rho U_{ac,i}^*$  is the streamwise component of the mass-flux perturbation that is produced by the incoming acoustic disturbance at the airfoil location (but in the absence of the airfoil). The quantity  $E_{\rho U}(Y; \omega, \beta_w + \beta_{ac}, R_{\delta^*})$  represents the local eigenfunction for the  $\rho U$  perturbation, which is assumed to have been normalized so that it has a maximum magnitude of unity across the boundary layer. The ‘‘coupling coefficient’’ function (Tam 1981, Goldstein 1985)  $C_{\rho U; \rho U}^{(j)}(\beta_w, \alpha_{ac}, \beta_{ac}, \omega, R_{\delta^*})$  then represents the ratio of the amplitude of the generated instability wave at  $X = 0$  to the amplitude of the incident acoustic wave; both amplitudes are measured in terms of the respective fluctuations in the streamwise mass flux  $\rho U$ , as indicated by the double subscript  $\rho U; \rho U$ .

When the geometry of the surface disturbance is more general than the harmonic form in (4a), the total unsteady fluctuation associated with the locally excited instability motion can be evaluated by integrating over the contributions from the different spanwise Fourier modes of the surface nonuniformity. (See Choudhari and Kerschen (1990) and Choudhari (1993).) Thus, if the nonuniformity has a periodic structure in the spanwise direction (e.g., that corresponds to a periodic array of suction holes), then the above sum will assume the form of a discrete Fourier series in the  $Z$  coordinate. On the other hand, if the nonuniformity is localized in both the streamwise and spanwise directions, then this sum will become an inverse Fourier integral in the  $\beta_{ins}$  plane.

Because of the bilinear nature of the acoustic scattering process, the coupling coefficient function can be written in a form that is similar to that in low-speed boundary layers, namely,

$$C_{\rho U; \rho U}^{(j)} = \epsilon_w^{(j)} \bar{\mathcal{F}}^{(j)}(\alpha_w) \Lambda_{\rho U; \rho U}^{(j)}(\omega, R_{\delta^*}, \alpha_{ac}, \beta_{ac}), \quad (6b)$$

where  $\alpha_w \equiv \alpha_{ins} - \alpha_{ac}$  and the cases  $j = s$  and  $j = t$  correspond to the receptivity induced by variations in the wall suction velocity and the wall temperature, respectively. The factor  $\epsilon_w^{(j)} \bar{\mathcal{F}}^{(j)}$  measures the amplitude of the Fourier harmonic  $(\alpha_w, \beta_w)$  of the surface suction or the surface temperature distribution. This particular Fourier component of the mean-flow disturbance is responsible for ‘‘tuning’’ the acoustic phase to that of

the generated instability mode. The efficiency function  $\Lambda_{\rho U; \rho U}^{(j)}$  is independent of the local geometry and is completely determined by the type of surface nonuniformity and other flow parameters such as the frequency  $\omega$  and wavenumbers  $\alpha_{ac}$  and  $\beta_{ac}$  of the incoming acoustic wave, and the local Reynolds number  $R_\delta^*$ . This type of decoupling between the geometry and efficiency factors, which was first pointed out by Goldstein (1985), is common to all receptivity mechanisms that involve a scattering of small-amplitude free-stream disturbances by weak surface inhomogeneities. As the numerical results in the following section demonstrate, the above decoupling enables (1) the study of the intrinsic features of each receptivity mechanism independent of the geometry involved and (2) the direct comparison of the receptivity caused by different types of surface nonuniformities, with the assumption that the spatial distributions for all nonuniformities are similar to each other (but otherwise arbitrary).

In (6), we used the perturbation in the streamwise mass flux to measure the amplitudes of both the input (i.e., acoustic) and the output (i.e., instability) waves. As noted by Choudhari and Streett (1991), the knowledge of  $C_{\rho U; \rho U}^{(j)}$  is adequate to determine the outcome of the localized receptivity process in any given case. However, the trends in the coupling-coefficient magnitude with respect to variation in the flow parameters can be substantially different if either or both of the wave amplitudes are measured in terms of a different physical quantity, such as the associated pressure fluctuation at the surface. The selection of the most appropriate physical quantity for measuring the amplitudes of the reference and the output waves is relatively less difficult in the case of incompressible boundary layers, particularly when these flows are two dimensional or axisymmetric. This is because the dynamics of the transition process in the above cases is dominated by velocity perturbations that are parallel to the mean flow.

The streamwise velocity perturbation is also easy to measure in a wind-tunnel experiment by using a hot-wire anemometer. Because the hot-wire response is actually a combined measure of the perturbations in both the velocity and the density at the measurement location, a natural extension of the above definition of wave amplitudes to compressible boundary layers is to specify the wave amplitudes in terms of the respective fluctuations in the streamwise mass flux. This choice was made by El-Hady (1991), who examined the effect of flow nonparallelism on

the growth of an instability wave. In studies of receptivity in compressible flows, the same choice of wave amplitudes is deemed convenient under many circumstances. However, situations do occur in which the pressure fluctuation produced by the incident acoustic wave is more appropriately used as the measure of the input-wave amplitude. This situation occurs, for instance, when one is studying the variation of the coupling coefficient with respect to the orientation of the incident acoustic wave because the  $\rho U$  perturbation associated with an incident wave of given sound pressure level (SPL) can vary dramatically as the angle of incidence is varied across its permitted range.

### 3. Numerical Results

For a parametric study, we choose to examine the receptivity of the boundary-layer flow past a semiinfinite, adiabatic flat plate. The stagnation temperature of the oncoming flow is held fixed at 311 K as the Mach number is varied. To start, we will consider the generation of a two-dimensional instability wave (by two-dimensional acoustic disturbances) in a subsonic boundary layer. Specifically, in section 3.1, we examine the influence of the free-stream Mach number on the coupling coefficients for receptivity that is produced through variations in both surface suction and surface temperature. Of particular interest is the comparison of the receptivity produced by the two types of LFC devices for a given extent of stabilizing influence on the incoming boundary layer. The influence of acoustic-wave orientation on the coupling coefficients is considered in section 3.2. Therein, we illustrate how the acoustic-signature field and the coupling coefficient in each case can at times be dramatically influenced by the refraction of the acoustic motion across the mean boundary layer. The cumulative effect of a series of suction or heating or cooling strips on the receptivity process is studied in section 3.3. In subsonic flows at sufficiently large Mach numbers, the spanwise length scale of the acoustic waves can become sufficiently short, whereby a three-dimensional instability wave can be excited even when the surface nonuniformity (i.e., suction or heating or cooling strip) is purely two dimensional. The excitation of three-dimensional instability waves by three-dimensional acoustic waves is examined in section 3.4. Finally, in section 3.5, the receptivity of a supersonic boundary layer is considered.

### 3.1 Influence of Mach Number on the Coupling Coefficient

In the first set of calculations, we consider the generation of two-dimensional instabilities near a suction (or heat-transfer) strip that corresponds to a uniform distribution of suction velocity (or temperature perturbation) across its width. The location of the strip is assumed to be at  $R \equiv R_{\delta^*}^{1/2} = 955$  at all Mach numbers. This choice results in a slightly different value of  $R_{\delta^*}$  at each Mach number. However, the use of  $R_{\delta^*}$  (i.e., the Reynolds number based on the distance from the leading edge) is more convenient for a flat-plate geometry. Moreover, because the range of Mach numbers considered here is limited, the accompanying variation in  $R_{\delta^*}$  is not large.

We assume that the orientation of the incident acoustic wave is held fixed at  $\theta_{ac} = 45^\circ$  as the Mach number is varied. Here,  $\theta_{ac}$  denotes the (clockwise) orientation of the wave-number vector of the incident acoustic wave with respect to the mean-flow direction. Thus, the range  $\theta_{ac} \in [0, \pi/2)$  corresponds to incident waves that travel downstream, whereas  $\theta_{ac} \in (\pi/2, \pi]$  denotes the range of upstream-traveling incident waves. The polar angle of incidence  $\theta_{ac}^p$  with respect to the surface normal is related to  $\theta_{ac}$  via  $\theta_{ac}^p = |\pi/2 - \theta_{ac}|$ . Note that in a wind-tunnel experiment it is perhaps easier to produce an acoustic wave that propagates downstream (as well as upstream in a subsonic flow) in a direction parallel to the plate. However, the choice  $\theta_{ac} = 45^\circ$  appears to be more general than  $\theta_{ac} = 0^\circ$  for assessing the values of the coupling coefficient. Subsequent calculations in which we examine the influence of acoustic-wave orientation on receptivity will demonstrate that the value of the efficiency function for an incident wave that propagates downstream (and upstream if the Mach number is small) can be easily related to the efficiency function for an incident wave that propagates along  $\theta_{ac} = 45^\circ$ .

The geometry factor for the suction or heat-transfer strip is given by

$$\bar{\mathcal{F}}^{(j)} = \frac{2^{1/2} \sin(\alpha_w d/2)}{\pi^{1/2} \alpha_w} \quad (7a)$$

where  $d$  is the (nondimensional) width of the strip. We have assumed that the amplitude of  $\mathcal{F}^{(j)}(X)$  is equal to unity for both  $j = s$  and  $j = t$ . We will focus our attention on the excitation of the instability mode that corresponds to the lower branch (to be indicated by subscript lb in this paper) of the neutral stability curve at  $R = 955$ .

In that case, (7a) shows that the geometry factor has its maximum magnitude when the width  $d$  of the suction or heating strip is given by

$$d = \frac{\pi}{\alpha_{w; \text{lb}}} \quad (\alpha_{w; \text{lb}} = \alpha_{ins; \text{lb}} - \alpha_{ac; \text{lb}}). \quad (7b)$$

To obtain the upper limit on the receptivity produced by a single strip, assume that the strip width is equal to the value given by (7b). Because the wave number  $\alpha_{ins; \text{lb}}$  of the neutral instability wave at  $R = 955$ , and the wave number  $\alpha_{ac; \text{lb}}$  of the incident acoustic wave vary with  $M$ , the total mass or heat flux across the width of the strip will also be a function of  $M$  with the above choice of strip width. This total-flux parameter is expected to determine the overall stabilizing influence of a suction (or heating) strip upon the boundary layer. As a result, the total ‘‘gain’’ from the suction or heating strip will vary to some extent with the Mach number. Nevertheless, the overall variation in  $\alpha_{w; \text{lb}}$  is relatively small at the assumed value of acoustic orientation ( $\alpha_{w; \text{lb}} \approx 0.13$  at  $M = 0$ , whereas  $\alpha_{w; \text{lb}} \approx 0.09$  at  $M = 0.99$ ). Therefore, the above choice of strip width appears to be reasonable from the standpoint of assessing the effect of free-stream Mach number on the coupling coefficient  $C_{\rho U; \rho U}^{(s)}$  that is likely to be measured in an experiment.

In figures 1(a) and 1(b), we have plotted the magnitudes of the normalized coupling coefficients  $\frac{C_{\rho U; \rho U}^{(s)}}{C_w^{(s)}}$  and  $\frac{C_{\rho U; \rho U}^{(t)}}{C_w^{(t)}}$  in the above case as functions of  $M$ . For both types of surface disturbances, the coupling-coefficient magnitude varies linearly with  $M$  as  $M \rightarrow 0$ . In other words, the compressibility correction to the coupling coefficient is  $O(M)$  in magnitude, which is significantly larger than the  $O(M^2)$  variation in the same limit in both the local stability properties (Ryzhov and Zhuk 1986, Smith 1989) and the characteristics of the mean-flow perturbation (Stewartson 1974). The  $O(M)$  variation in the receptivity properties is mainly caused by a comparable variation in the acoustic-signature field as  $M \rightarrow 0$  and can be explained in the following manner.

Goldstein (1985) and Ruban (1985) showed that the receptivity near the lower branch location is mainly concentrated in a thin subregion of the mean boundary layer that occupies the region close to the surface. Because the acoustic wavelength at the frequency and in the range of Mach numbers under consideration is asymptotically larger than the thickness of the mean boundary layer, the acoustic pressure fluctuation varies very little across the

boundary layer. Moreover, the zero-normal-flow condition at the surface causes the reflected pressure wave to be in phase, locally, with the incident wave. As a result, the pressure fluctuation near the surface is twice as large as the pressure perturbation associated with the incident wave alone. The pressure perturbation drives a Stokes shear wave in the viscous wall layer, which is scattered by the local mean-flow perturbation to produce the instability wave. The profile of the Stokes wave is independent of the flow Mach number, the acoustic orientation  $\theta_{ac}$ , and the mean boundary-layer properties. As a consequence, the coupling coefficient is simply proportional to the amplitude  $U_{st}$  of the Stokes wave, which differs from the streamwise velocity perturbation associated with the incident acoustic wave by a factor given by

$$\frac{U_{st}}{U_{ac;i}} \sim \frac{2}{1 + M \cos \theta_{ac}} \quad (u_{ac;i} = M \cos \theta_{ac} P_{ac;i}). \quad (8)$$

The factor 2 in the numerator of the right-hand-side in (8) accounts for the reinforcement of the Stokes-wave amplitude by the reflected acoustic wave, whereas the factor  $1 + M \cos \theta_{ac}$  in the denominator is attributed to the difference in inertial forces in the wall layer and in the local free-stream region. The other reason for the  $O(M)$  variation in the coupling coefficient as  $M \rightarrow 0$  is that the receptivity is correlated with the amplitude of the streamwise velocity perturbation produced by the Stokes wave; the coupling coefficient in figures 1(a) and 1(b) is based on the mass-flux perturbation associated with the incident wave. The amplitudes of the acoustic perturbations in velocity and mass flux differ by an  $O(M)$  amount that corresponds to the extent of density perturbation produced by the acoustic wave.

The coupling coefficient for both types of surface nonuniformities decreases as the free-stream Mach number is increased. Throughout the range of Mach numbers considered, the ratio  $|C_{\rho U; \rho U}^{(s)}|/|C_{\rho U; \rho U}^{(t)}|$  of the coupling coefficients is in the range of approximately 150 – 200 times the ratio  $\epsilon_w^{(s)}/\epsilon_w^{(t)}$  of the corresponding surface-disturbance amplitudes. Note that receptivity that is induced by a given distribution of surface suction or surface temperature is generally an undesirable by-product, or “cost,” of using that particular type of LFC device. Therefore, in order to compare the costs involved in using surface suction and surface heat transfer for LFC, it is necessary to adjust the ratio  $\epsilon_w^{(s)}/\epsilon_w^{(t)}$  of amplitude parameters in such a way that the gain in stability (i.e., the

increase in transition Reynolds number) is the same in both cases.

Because the effect on stability of a single heating or cooling strip is highly sensitive to the location of the strip (Masad and Iyer, 1993), we assume that the suction and the heat-transfer strip under consideration is just one out of many such strips that comprise the LFC system. One would expect that the effect on stability of this type of configuration will be analogous to that of continuous suction or cooling at a suitably modified level. A comparison of the results in figures 12(a) and 14(a) in Masad and Iyer (1993) shows that in order to achieve an identical increase in the transition Reynolds number for both types of LFC, the surface-temperature perturbation  $\epsilon_w^{(t)}$  needs to be approximately 2150 times larger than the suction parameter  $\epsilon_w^{(s)}$ . The above estimate corresponds to the linearized limit employed in this paper, however the ratio  $\epsilon_w^{(t)}/\epsilon_w^{(s)}$  was found to increase further as the respective amplitudes were increased beyond the linear range.

For the case of  $\epsilon_w^{(t)}/\epsilon_w^{(s)} = 2150$ , the coupling coefficient for the heat transfer strip in figure 1b will be almost 11 to 15 times larger than the coupling coefficient for the receptivity produced by the suction strip. The lower ratios in the above range correspond to smaller Mach numbers, whereas the higher values correspond to the transonic range of Mach numbers. In section 3.2, we will allow both the frequency parameter and the orientation of the incident wave to vary, but keep the Mach number fixed at  $M = 0.9$ . The results obtained for these cases indicate that the ratio of the coupling coefficients for the two types of LFC devices varies with  $\omega$  and  $\theta_{ac}$ , but nowhere to the extent where it will affect the above conclusion concerning the qualitative comparison of their respective magnitudes. Note that the estimate that  $\epsilon_w^{(t)}/\epsilon_w^{(s)} = 2150$  for equal gains in stability was based on the results obtained in the low-Mach-number limit, but we do not expect it to change significantly over the Mach-number range considered. Of course, it needs to be seen at what values of  $\epsilon_w^{(t)}$  and  $\epsilon_w^{(s)}$  the linearized theory becomes inappropriate.

### 3.2 Influence of Acoustic-Wave Orientation

Now we examine the influence of the acoustic-wave orientation  $\theta_{ac}$  on the receptivity produced by both types of surface disturbances. Toward this purpose, we consider the variation with  $\theta_{ac}$  in the respective coupling coefficients at a fixed Mach number. The location of the strip and the acoustic frequency parameter are the same as the corresponding values in figures 1(a) and 1(b). How-

ever, the strip geometry in (7b) is discarded in favor of a narrow suction and heating/cooling strip that is approximated by the distribution  $\mathcal{F}^{(j)}(X) = (2\pi)^{-1/2}\delta(X)$ . Recall from (6b) that the coupling coefficient for this geometry is given precisely by the relevant efficiency function  $\Lambda^{(j)}$ . The reason for choosing the narrow-strip geometry is that its Fourier spectrum is uniform across the wave-number range of interest and, hence, is independent of the wave number  $\alpha_{w,lb}$  at which the geometry factor  $\bar{\mathcal{F}}^{(j)}$  is evaluated. At sufficiently large Mach numbers, the acoustic wave number  $\alpha_{ac}$  varies significantly with  $\theta_{ac}$ . Consequently, the choice of the geometry in (7b) will lead to significant variation in  $\alpha_{w,lb}$  and hence in the width of the strip as the independent parameter  $\theta_{ac}$  is varied across its range. This problem does not arise in the narrow-strip limit. Moreover, as shown by Kerschen and Choudhari (1985) (see, also, Choudhari 1992), a narrow suction strip will result in the maximum coupling coefficient for  $\omega = \omega_{lb}$ , provided that the total suction rate across the strip is kept fixed as the strip width is varied.

Because of the variation in  $\alpha_{ac}$  with  $\theta_{ac}$ , the  $\rho U$  perturbation produced by an incident acoustic wave of given SPL also varies significantly as  $\theta_{ac}$  is varied across  $[0, \pi]$ . In fact, for  $M < 1$ , the  $\rho U$  perturbation becomes zero at a critical angle of incidence. The critical angle is given by  $\theta_{ac} = \cos^{-1}(-M)$  and lies in the range  $(\pi/2, \pi)$  (i.e., in the range of upstream-inclined acoustic waves). Therefore, in this section,  $P_{ac,i}$  is kept fixed as  $\theta_{ac}$  is varied (rather than fixing  $(\rho U)_{ac}$  as in figures 1(a) and 1(b) of the previous section).

The solid curves in figures 2(a), 2(b), and 2(c) illustrate the variation in the efficiency function  $|\Lambda_{\rho U;P}^{(s)}(\theta_{ac})|$  at  $M = 0.1$ , 0.5, and 0.9, respectively. In each case, the efficiency function has been normalized by its value for  $\theta_{ac} = 0$  (i.e., for an incident wave that propagates parallel to the mean-flow direction). Because of this normalization, the results plotted are actually independent of the physical quantity that is used to measure the instability-wave amplitude. In addition, for  $M = 0.1$  and 0.5, the acoustic wave number is uniformly small as compared to  $\alpha_{ins,lb}$ . Therefore, in general, it will not influence the magnitude of the geometry factor  $\bar{\mathcal{F}}^{(j)}(\alpha_{w,lb})$  to a significant extent, as a result of which the results in figures 2(a) and 2(b) also approximate the ratio of the coupling coefficients for the strip geometry defined by (7b). At each selected Mach number, the highest value of the efficiency-

function magnitude corresponds to an incident wave that is inclined in the upstream direction. At sufficiently small Mach numbers (figure 2(a)), this maximum corresponds to an incident wave that travels in the direction that is nearly opposite to the direction of the mean flow. Moreover, in all three cases, the ratio of the maximum efficiency function magnitude to that at  $\theta_{ac} = 0$  is nearly equal to the corresponding ratio of the Stokes-wave amplitudes in the viscous sublayer, which is indicated in figures 2(a) through 2(c) by the curve that contains symbols. In fact, the entire  $|\Lambda_{\rho U;P}^{(s)}(\theta_{ac})|/|\Lambda_{\rho U;P}^{(s)}(\theta_{ac} = 0)|$  curve correlates with the ratio of Stokes-wave amplitudes, which was obtained from (8).

The maximum of the ratio of the Stokes-wave amplitudes at any given Mach number always corresponds to the upstream-traveling mode, and it increases rapidly with the free-stream Mach number. Although the maximum of the efficiency-function curve also increases with  $M$ , it increases relatively less rapidly as  $M$  approaches the transonic range (figure 2c). Moreover, this maximum corresponds to an incidence angle of  $\theta_{ac} \approx 145^\circ$  at  $M = 0.9$ , and the efficiency-function magnitude decreases rapidly as  $\theta_{ac}$  is increased further. Although a similar behavior is also noted at  $M = 0.5$ , it is most prominent in the transonic case at  $M = 0.9$ .

The cause for the deviation of the efficiency-function curve from that predicted by (8) was traced to the variations in the acoustic pressure field across the mean boundary layer, which result in a weaker acoustic-signature field within the viscous sublayer next to the surface. As remarked in section 3.1, the surface pressure coefficient  $\mathcal{C}_P \equiv P_{ac}(Y = 0)/P_{ac,i}$  is equal to 2 at nearly all values of  $\theta_{ac}$  when the Mach number is sufficiently small. However, this picture begins to change as the Mach number  $M$  becomes larger. This change is caused by a decrease in the acoustic wavelength (relative to the boundary-layer thickness) that accompanies the increase in  $M$  and leads to a significant refraction of the incident and the reflected waves across the mean boundary layer. In effect, the refraction process modifies the perfect in-phase relationship (i.e., a constructive interference) between the incident and reflected waves near the surface. This modification leads to a reduction in  $|\mathcal{C}_P|$  and also alters the nature of velocity fluctuations close to the surface. At a fixed value of the frequency parameter, the acoustic wavelength is relatively shorter for the upstream-travelling waves and, hence, the refraction by the mean boundary layer is more

significant for  $\theta_{ac} > \pi/2$ . As an example, consider the frequency parameter that corresponds to the lower branch mode at  $R = 955$  and  $M = 0.9$ . At this frequency, the shortest acoustic length scale (defined as one-quarter of the acoustic wavelength) is approximately five times the displacement thickness of the mean boundary layer (i.e., only about 1.6 times larger than the boundary-layer thickness based on 99.9 percent of the local free-stream speed). The effect of transverse pressure variations in transonic boundary layers has also been noted by Ryzhov (1993); however, this work examined the stability of boundary layers rather than their receptivity to acoustic disturbances.

To check on our numerical calculations, we also computed  $\mathcal{C}_P$  as a function of  $\theta_{ac}$  at Reynolds numbers of  $R = 1910$  (i.e.,  $R = 2.0 * 955$ ) and  $R = 3820$  (i.e.,  $R = 4.0 * 955$ ) for the same value of the nondimensional frequency parameter  $\omega$  considered in figure 3(a) at  $R = 955$ . Because the mean boundary-layer profile is self-similar, the  $\mathcal{C}_P$  versus  $\theta_{ac}$  variation at all three Reynolds numbers was graphically indistinguishable. As a result, a purely inviscid calculation such as that carried out by Duck (1990) for  $M > 1$  is also expected to yield the same result for the acoustic-field signature.

As long as the efficiency function correlates with the amplitude of the Stokes shear wave, its dependence on  $\theta_{ac}$  is nearly identical for both types of surface nonuniformities. (See figures 3a through 3c for the variation of  $|\Lambda_{\rho U; P}^{(t)}|$  with  $\theta_{ac}$ .) However, if the acoustic-signature field becomes nontrivial because of the refraction effect at the higher Mach numbers, then the dependence of  $|\Lambda_{\rho U; P}^{(j)}|$  on  $\theta_{ac}$  tends to be different for the different type of surface nonuniformities. For example, the maximum values of  $|\Lambda_{\rho U; P}^{(j)}(\theta_{ac})|/|\Lambda_{\rho U; P}^{(j)}(\theta_{ac} = 0)|$  in figures 2(c) and 3(c) are equal to 2.2 and 3.6, respectively, for  $j = s$  and  $j = t$ . Similarly, in a companion study that deals with the receptivity induced by surface-geometry variations, we have found that the corresponding peak value for the geometry-induced receptivity is equal to approximately 8.1. Note that the finding of a somewhat larger peak ratio in the case of temperature-induced receptivity as compared to that for the suction-induced receptivity tends to support our earlier remarks (section 3.1) in regard to the relative strength of those two receptivity mechanisms.

The results in figures 2 and 3 can also be applied to predict the expected value of the efficiency function  $\Lambda_{\rho U; P}^{(j)}$  (i.e., the expected value of the coupling coefficient

in the narrow-strip limit) for the case where the angle of acoustic incidence  $\theta_{ac}$  is unknown, but has an equal probability of assuming any value in the range  $[0, \pi]$ . At  $M = 0.9$ , the expected magnitude of  $\Lambda_{\rho U; P}^{(j)}$  is predicted to be larger than  $|\Lambda_{\rho U; P}^{(j)}(\theta_{ac} = 0)|$  by a factor of approximately 1.07 for  $j = s$  and 1.54 for  $j = t$ . These factors are considerably smaller than the common factor 6.15 that would have been predicted on the basis of (8).

Thus far, we have discussed the excitation of the instability wave that corresponds to the lower branch mode at the location of the strip. Figures 4(a) and 4(b) depict the variation in the efficiency functions  $|\Lambda_{\rho U; P}^{(j)}|$  at  $R = 955$  as the acoustic frequency parameter is varied while the angle  $\theta_{ac}$  remains fixed at a given value. Note that a comparison of  $|\Lambda_{\rho U; P}^{(j)}|$  for  $j = s$  and  $j = t$  is also equivalent to the comparison of the respective coupling coefficients for an arbitrary distribution  $\mathcal{F}^{(j)}(X)$ , provided that  $\mathcal{F}^{(s)}(X) = \mathcal{F}^{(t)}(X)$ . The abscissa in figures 4a and 4b corresponds to  $f \equiv \frac{\omega^* \nu^*}{U_\infty^*} \equiv \omega/R\delta^*$  and results have been plotted for a set of selected values for  $\theta_{ac}$ . For reference, the variation with  $f$  in the spatial growth rate  $-\text{Im}(\alpha)$  and the phase speed  $c_{ins} \equiv \omega/\text{Re}(\alpha)$  is also indicated in each plot.

For suction-induced receptivity, the magnitude of the efficiency function increases as the frequency parameter is reduced. Of course, the low-frequency modes will have to undergo an exponential decay before they reach their respective lower branch locations. Therefore, the highest effective amplitude at the lower branch location will correspond to a frequency parameter that is somewhat smaller than the lower branch frequency. Alternatively, if one is interested in the excitation of the instability wave at a given frequency, then the most dangerous location for a narrow suction strip will be slightly upstream of the lower branch. For any given  $\theta_{ac}$ , the behavior of the efficiency function curve  $|\Lambda_{\rho U; P}^{(t)}|$  is somewhat different from that of  $|\Lambda_{\rho U; P}^{(s)}|$ . This difference is such that in the range of unstable frequencies it tends to enhance the ratio  $|\Lambda_{\rho U; P}^{(t)}|/|\Lambda_{\rho U; P}^{(s)}|$  as compared to the value of this ratio for the lower branch mode. On the other hand, the rapid rise in  $|\Lambda_{\rho U; P}^{(s)}|$  in the low-frequency regime will reduce the ratio of coupling coefficients to a small extent. Finally, we observe that for both types of LFC devices, the angle of acoustic incidence that leads to the most efficient excitation of the instability wave of a given frequency tends to decrease somewhat as  $f$  is increased. However, in general, the above orientation always corresponds to

an upstream-travelling acoustic wave.

### 3.3 Receptivity Produced by an Array of Suction or Heating/Cooling Strips

Because of the weak-surface-nonuniformity assumption utilized in this paper, the receptivity predictions for an individual suction or heating strip can easily be extended to an array of strips with an arbitrary distribution of suction velocity or surface temperature. The general framework to extend the Goldstein-Ruban theory for localized receptivity to the case of receptivity produced by distributed surface nonuniformities was described by Choudhari and Streett (1990, 1991) and in further detail by Choudhari (1993a,b). Basically, the efficiency function for localized receptivity is utilized as a local influence function in the latter case. (This idea was originally proposed by Tam (1981) in a related context.) The net receptivity is obtained by integrating over the contributions from each individual subregion across the length of the region of nonuniformities.

As shown by Zavol'skii *et al.* (1983), Tumin and Fedorov (1983), and Choudhari (1993a,b), the above integration process must include the effect of interference between the instability waves that are generated in different parts of the overall region of receptivity. The outcome of the interference process is determined by the geometry of the surface nonuniformity and by the variations in the wave numbers  $\alpha_{ins}$  and  $\alpha_{ac}$  across the region of receptivity. In particular, when a uniform suction (or heat flux) is applied through an array of equidistant strips of uniform width, Choudhari (1992) showed that most of the receptivity is actually produced by the strips that are located in the vicinity of the lower branch location. The ratio of the effective coupling coefficient  $C_{array}^{(j)}$  for the array (which measures the effective amplitude of the generated instability motion near the lower branch location) to the local coupling coefficient  $C_{local}^{(j)}$  for a single strip at the lower branch location is given by

$$\mathcal{R}_{array} \equiv \frac{C_{array}^{(j)}}{C_{local}^{(j)}} = \frac{|\alpha_{w;lb}|}{\tilde{\mathcal{F}}^{(j)}(\alpha_{w;lb})\sqrt{i\pi\tilde{D}_\alpha}} \sum_{n=1}^{\infty} \tilde{\mathcal{F}}^{(j)}(n\alpha_{w;lb}) \exp\left[-\frac{(n\alpha_{w;lb} + \alpha_{ac;lb} - \alpha_{ins;lb})^2}{i\tilde{D}_\alpha}\right]. \quad (9a)$$

Here  $\alpha_w(R_{\delta^*}) \equiv \alpha_w^* \delta^*(R_{\delta^*})$  denotes the fundamental wave number of the periodic suction (or temperature) distribution, and the factor  $\tilde{D}_\alpha$  is a measure of how rapidly the unsteady forcing on the right-hand side of (3) (which

is produced by the bilinear interaction between the free-stream and surface disturbances) becomes detuned, or “desynchronized,” with respect to the phase of the instability mode. For a flat plate boundary layer, the desynchronization factor is given by

$$\tilde{D}_\alpha \equiv \left(\frac{R_{\delta^*_{lb}}^2}{R_{l^*_{lb}}}\right) D_\alpha \quad \left[D_\alpha = \left(\alpha'_{ins;lb} - \frac{\alpha_{ins;lb}}{R_{\delta^*_{lb}}}\right)\right] \quad (9b)$$

where the primes denote differentiation with respect to  $R_{\delta^*}$ , and the subscript lb indicates evaluation at the lower branch location  $R_{\delta^*} = R_{\delta^*_{lb}}$ , as mentioned previously. In an accelerating or decelerating free stream, the expression for  $D_\alpha$  will also incorporate the additional detuning (or tuning) because of the variations along the streamwise direction in the physical wave number of the acoustic wave. Note that the ratio in (9a) is independent of the physical quantity in terms of which the amplitudes of the input and the output waves are measured, provided only that the same measure is adopted for both types of configurations. As a result, we have dropped the corresponding subscripts on  $C^{(j)}$  in both the numerator and the denominator.

To supplement the results of section 3.1 on the receptivity induced by a single strip, we can examine the upper limit on the receptivity produced by an array of strips. For the strip configuration defined in (7), we expect that the maximum receptivity will occur when  $\alpha_{w;lb} = \alpha_{ins;lb} - \alpha_{ac;lb}$ . In that case, the maximum value of the ratio in (9a) will be given by

$$\mathcal{R}_{array;max} = \left|1 - \frac{\alpha_{ac;lb}}{\alpha_{ins;lb}}\right| \mathcal{R}_D \quad (9c)$$

where

$$\mathcal{R}_D = \frac{\alpha_{ins;lb}}{\sqrt{i\pi\tilde{D}_\alpha}}. \quad (9d)$$

The factor  $\mathcal{R}_D$  is independent of  $\theta_{ac}$  when the free stream is uniform. However, the ratio  $\mathcal{R}_{array;max}$  is a function of the acoustic-wave orientation because of the additional factor  $\mathcal{R}_\alpha \equiv 1 - \frac{\alpha_{ac;lb}}{\alpha_{ins;lb}}$  ( $= 1 - \frac{c_{ins} M \cos \theta_{ac}}{1 + M \cos \theta_{ac}}$  for a two-dimensional acoustic wave) that appears on the right hand side of (9c). An analogous factor is also present in the case of receptivity to convected free-stream disturbances. However, for convected disturbances, the factor  $\mathcal{R}_\alpha$  is independent of the disturbance structure along the surface-normal direction (e.g., the orientation of the wave-number vector if a single Fourier mode of the convected perturbation is considered). Because of an oversight, the factor  $\mathcal{R}_\alpha$  was omitted in (4a) of Choudhari

(1994) and, also, in the estimate for distributed receptivity presented in Choudhari and Streett (1993), which led to the an overprediction of the ratio  $\mathcal{R}_{array; \max}$  in those works.

Not only does  $\mathcal{R}_\alpha$  depend on the orientation of the incident disturbance in the case of free-stream acoustic waves, but can lead to either an increase or a decrease in the magnitude of  $\mathcal{R}_{array; \max}$ , depending on  $\theta_{ac}$ . For downstream travelling waves  $\alpha_{ac; lb}$  is positive, which implies that  $|\mathcal{R}_\alpha| < 1$  for those waves. On the other hand,  $\alpha_{ac; lb}$  is negative for upstream travelling waves, and can assume rather large values at transonic Mach numbers. This will lead to a substantial increase in the magnitude of  $\mathcal{R}_{array; \max}$ . The physical explanation for the effect of  $\mathcal{R}_\alpha$  on the effective coupling coefficient for distributed receptivity is as follows. The length scale of distributed receptivity is fixed by the desynchronization factor  $\tilde{D}_\alpha$ . Therefore, it does not vary with  $\theta_{ac}$  in the case of a flat-plate boundary layer. An increase or decrease in  $\alpha_{w; lb} = \alpha_{ins; lb} - \alpha_{ac; lb}$  then corresponds to a decrease or increase in the spacing between an adjacent pair of strips. The latter, in turn, implies an increase or decrease in the number of strips that lie within the (fixed) length scale of distributed receptivity and, hence, contribute to its cumulative effect.

In the context of the conceptual experiment considered in figures 1(a) and 1(b), we note that for  $\theta_{ac} = 45^\circ$  the factor  $\mathcal{R}_\alpha$  varies from 1.0 at  $M = 0$  to approximately 0.87 at  $M = 0.99$ . (Because the value of  $\mathcal{R}_\alpha$  is nearly equal to unity in this case, the ratio  $\mathcal{R}_{array; \max}$  could even be approximated by the factor  $\mathcal{R}_D$ .) The magnitude of  $\mathcal{R}_D$  at a lower branch Reynolds number of  $R = 955$  has been plotted in figure 5 as a function of  $M$ . The magnitude of  $\mathcal{R}_D$  decreases from 9.3 at  $M \rightarrow 0$  to approximately 7.3 as  $M \rightarrow 1.0$ . Therefore, at  $\theta_{ac} = 45^\circ$ , the ratio  $|\mathcal{R}_{array; \max}|$  will decrease from 9.3 to 6.3 across the range of subsonic Mach numbers. By combining this estimate with the results of figures 1(a) and 1(b), we can conclude that the effective coupling coefficients  $C_{\rho U; \rho U}^{(j)}$  for distributed receptivity will exhibit the same trend, as the Mach number is varied, as that of the respective local coupling coefficient for an individual strip (figures 1(a) and 1(b)).

### 3.4 Excitation of Three-Dimensional Instability Waves

The results of section 3.2 demonstrate how the decrease in the acoustic wavelength as  $M$  increases can have

a significant impact on the acoustic-signature field and on the magnitude of the coupling coefficients. Another consequence of the decreasing acoustic wavelength at  $O(1)$  Mach numbers is that even three-dimensional instability waves can be excited near a two-dimensional distribution of surface nonuniformities if the free-stream disturbance has a suitable azimuthal orientation. In figure 6(a), we have plotted the azimuthal angle  $\phi_{ins} \equiv \arctan\left(\frac{\beta_{ins}}{\text{Real}(\alpha_{ins})}\right)$  of the generated instability wave as a function of the azimuthal orientation  $\phi_{ac}$  of the incident acoustic wave. The Mach number chosen for this calculation is equal to 0.9, and the values of  $R$  and  $\omega$  are the same as the corresponding values at  $M = 0.9$  in figure 1(c). The polar angle of incidence  $\theta_{ac}^p = |\pi/2 - \theta_{ac}|$  is held fixed, and  $\phi_{ac}$  is varied across the range  $0 < \phi_{ac} < \pi$ . When  $\phi_{ac}$  is an acute angle, the incident wave propagates downstream; for obtuse azimuthal orientations ( $\phi_{ac} > \pi/2$ ), the incident wave travels upstream. Thus, the case  $\theta_{ac}^p = 55^\circ$  and  $\phi_{ac} = 180^\circ$  corresponds to the two-dimensional wave with  $\theta_{ac} = 145^\circ$  in figures 1(c) and 3(c), which leads to the highest value of the normalized coupling coefficient for both  $j = s$  and  $j = t$ .

For  $\omega = \omega_{lb}$  at  $R = 955$ , instability waves with  $\phi_{ins}$  less than approximately  $35^\circ$  can be excited near a two-dimensional surface nonuniformity. (See figure 6(a).) The maximum possible value of  $\phi_{ins}$  tends to increase as  $\theta_{ac}^p$  is increased, so that the above-mentioned upper limit on  $\phi_{ins}$  is realized when the incident wave propagates parallel to the plate surface. At any given  $\theta_{ac}^p$ , the same instability mode can be excited by a pair of acoustic waves that corresponds to two different values of  $\phi_{ac}$ . When  $\theta_{ac}^p$  is small, the  $\phi_{ins}$  curve is roughly symmetric with respect to  $\phi_{ac} = \pi/2$ . As a consequence, the wave-number vectors of two acoustic waves that excite the same instability mode are nearly symmetric with respect to the spanwise direction. As  $\theta_{ac}^p$  is increased, the behavior of  $\phi_{ins}$  becomes increasingly asymmetric about  $\phi_{ac} = \pi/2$ . Therefore, both incident waves, which excite an instability mode that corresponds to  $\phi_{ins}$  in the vicinity of its maximum, are upstream-travelling waves. The variation in the efficiency-function magnitudes for the two types of surface disturbances is shown in figures 6(b) and 6(c), respectively. Interestingly enough, the efficiency function at  $\theta_{ac} = 55^\circ$  and  $85^\circ$  actually tends to zero near some critical azimuthal orientation that corresponds to an upstream-inclined acoustic wave.

### 3.5 Receptivity at Low Supersonic Speeds

At subsonic Mach numbers, the angle  $\theta_{ac}$  of a two-dimensional incident wave can be varied continuously from 0 to  $\pi$  by varying its wave number  $\alpha_{ac}$  in the streamwise direction. However, for  $M > 1$ , the acoustic dispersion relation for a plane wave allows two disjointed sets of modes. The so-called fast mode is analogous to the acoustic waves in a subsonic flow, except that the angle of incidence for a fast acoustic mode in a supersonic stream is constrained to the range  $\theta_{ac} \in [0, \pi - \arccos(\frac{1}{M})]$  instead of the complete range  $[0, \pi]$  that is relevant at the subsonic Mach numbers. The excluded range of angles gets folded back to the range  $(-\arccos(\frac{1}{M}), 0)$  that the slow mode occupies. The slow mode has a critical layer within the mean boundary layer and is, therefore, unique to the supersonic range of Mach numbers. The solid curves in figures 7(a) and 7(b) illustrate the variation in the magnitudes of the efficiency functions  $|\Lambda_{\rho u; P}^{(s)}|$  and  $|\Lambda_{\rho u; P}^{(t)}|$  as  $\theta_{ac}$  is varied for both the fast and the slow acoustic modes in the boundary-layer flow at  $M = 1.2$ . Again, the location of the LFC device is chosen to be  $R = 955$ , and the frequency parameter corresponds to  $\omega \approx 0.033$ , which is close to the lower branch frequency predicted by the quasi-parallel stability theory. Note that the effect of non-parallelism becomes increasingly significant (in terms of determining the growth rate of a two-dimensional instability wave) as one crosses over the transonic regime into the supersonic range (Smith 1989, Ryzhov and Savenkov 1990). However, the leading-order eigenfunction is always determined by the quasiparallel theory (Fedorov and Khokhlov 1991); hence, the application of the present receptivity theory is feasible in this particular case.

Figures 7(a) and 7(b) show that the efficiency functions for the slow acoustic mode do not correlate with the behavior predicted by (8) (indicated by the curve with symbols). In fact, even the results for the fast mode show substantial deviation from the analytical prediction as  $\theta_{ac}$  becomes large. The highest value of the normalized coupling coefficient occurs for a fast mode that is incident at  $\theta_{ac} \approx 135^\circ$  in both cases. However, its magnitude for temperature-induced receptivity ( $\approx 4.25$ ) is much larger than that for the suction-induced receptivity ( $\approx 1.5$ ). The maximum coupling coefficient for a slow acoustic mode is smaller than the maximum for the fast mode in this particular case. However, this trend is not always the case; because an opposite trend was encountered in an analogous set of calculations at  $M = 1.6$ .

### 4. Concluding Remarks

The Goldstein-Ruban theory was extended in this paper to develop theoretical predictions for the acoustic receptivity produced by two-dimensional variations in the surface suction velocity and in the surface temperature. The receptivity mechanism that is related to mean-flow variations induced by these laminar flow control (LFC) devices is likely to be stronger when surface heating or cooling is used for LFC (in comparison with the case where surface suction is used). The orientation of the acoustic wave can have a significant impact on the magnitude of the coupling coefficient in both cases. Moreover, at the larger subsonic Mach numbers, this influence is rather nontrivial for upstream-oriented acoustic waves, which produce the highest receptivity at a given sound pressure level (SPL). Moreover, in the above speed range, the effect of acoustic-wave orientation is different for the different types of surface nonuniformities. Of course, the predictions developed in this study are limited to small-amplitude surface nonuniformities, and further study is required to identify the range of validity for the linearized approximation, particularly in the range of transonic Mach numbers.

The calculations also illustrate the influence of acoustic-wave orientation on the receptivity at supersonic Mach numbers; however, a more detailed parametric study is necessary to pinpoint the receptivity characteristics in this speed range, in particular because three-dimensional instability waves become more important at these Mach numbers. Such calculations will enable the assessment of the importance of receptivity near the leading edge and of that produced by the surface nonuniformities.

Finally, the study demonstrates the sensitive parameter dependence of acoustic receptivity in compressible boundary layers. This dependence will make it particularly difficult to predict the receptivity in actual applications and hence to predict the location of transition on a more rational basis.

### Acknowledgements

Financial support for the first author was provided by the Theoretical Flow Physics Branch at the NASA Langley Research Center, Hampton, VA 23681, under contract number NAS1-20059. The assistance of Dr. Surya Dinavahi and Dr. Gordon Erlebacher in developing the *Mathematica* code that was used to check the equations in the Appendix is greatly appreciated. In addition, the author acknowledges the useful discussions with

Dr. Jamal Masad in regard to the comparison between LFC techniques based on surface suction and surface heat transfer. Thanks are also due to Ms. Jonay Campbell for editing this manuscript.

### References

- Choudhari, M., 1992, "Distributed Acoustic Receptivity in Laminar Flow Control Configurations," NASA CR-4438 (see also: *Phys. Fluids*, Vol. 4, No. 2, 1994).
- Choudhari, M., 1993a, "Boundary-Layer Receptivity due to Distributed Surface Imperfections of a Deterministic or Random Nature," *Theoretical and Computational Fluid Dynamics*, Vol. 4, No. 3, pp. 187-212 (see also: NASA CR-4439, May 1992).
- Choudhari, M., 1993b, "Roughness-Induced Generation of Crossflow Vortices in Three-Dimensional Boundary Layers," NASA CR-4505 (see also: *Theor. and Comp. Fluid Dyn.*, Vol. 5, pp. 1-31, Feb. 1994).
- Choudhari, M., 1994, "Localized and Distributed Boundary Layer Receptivity to Convected Unsteady Wake in Free Stream," NASA CR-4578.
- Choudhari, M. and Kerschen, E. J., 1990, "Instability Wave Patterns Generated by Interaction of Sound Waves With Three-Dimensional Wall Suction or Roughness," AIAA Paper 90-0119.
- Choudhari, M. and Streett, C. L., 1990, "Boundary Layer Receptivity Phenomena in Three-Dimensional and High-Speed Boundary Layers," AIAA Paper 90-5258.
- Choudhari, M. and Streett, C. L., 1991, "A Finite Reynolds Number Approach for the Prediction of Boundary Layer Receptivity in Localized Regions," NASA TM-102781 (see also: *Phys. Fluids A*, Vol. 4, pp. 2495-2514, 1992).
- Duck, P. W., 1990, "The Response of a Laminar Boundary Layer in Supersonic Flow to Small-Amplitude Progressive Waves," *J. Fluid Mech.*, Vol. 219, pp. 423-448.
- El-Hady, N. M., 1991, "Nonparallel Instability of Supersonic and Hypersonic Boundary Layers," *Phys. Fluids A*, Vol. 3, No. 9, pp. 2164-2178.
- Fedorov, A. V. and Khokhlov, A. P., 1991, "Excitation of Unstable Modes in a Supersonic Boundary Layer," *Izv. Akad. Nauk SSSR, Mekh. Zhid. i Gaza*, No. 4, pp. 67-74.
- Fedorov, A. V. and Khokhlov, A. P., 1993, "Excitation of Unstable Modes in a Supersonic Boundary Layer," In *Transitional and Turbulent Compressible Flows*, FED-Vol. 151, ASME, NY, pp. 1-13.
- Gaponov, S. A., 1985, "On the Development of Disturbances in Nonparallel Supersonic Flows," In *Laminar-Turbulent Transition* (IUTAM Symp., Novosibirsk, Russia), Springer Verlag, Berlin, pp. 581-588.
- Goldstein, M. E., 1983, "The Evolution of Tollmien-Schlichting Waves near a Leading Edge," *J. Fluid Mech.*, Vol. 127, pp. 59-81.
- Goldstein, M. E., 1985, "Scattering of Acoustic Waves into Tollmien-Schlichting Waves by Small Streamwise Variations in Surface Geometry," *J. Fluid Mech.*, Vol. 154, pp. 509-529.
- Goldstein, M. E., Leib, S., and Cowley, S., 1987, "Generation of Tollmien-Schlichting Waves on Interactive Marginally Separated Flows," *J. Fluid Mech.*, Vol. 181, pp. 485-518.
- Goldstein, M. E., and Hultgren, L. S., 1989, "Boundary Layer Receptivity to Long-Wave Free-Stream Disturbances," *Ann. Rev. Fluid Mech.*, Vol. 21, pp. 137-166.
- Huerre, P. and Monkewitz, P. A., "Local and Global Instabilities in Spatially Developing Flows," *Ann. Rev. Fluid Mech.*, Vol. 22, pp. 473-537.
- Kendall, J., 1975, "Wind Tunnel Experiments Relating to Supersonic and Hypersonic Boundary Layer Transition," *AIAA J.*, Vol. 13, pp. 240-249.
- Kerschen, E. J., 1989, "Boundary Layer Receptivity," AIAA Paper 89-1109.
- Kerschen, E. J., and Choudhari, M., 1985, "Boundary Layer Receptivity at a Suction Surface-Hard Wall Junction," *Bull. Am. Phys. Soc.*, Vol. 30, No. 10, p. 1709.
- Kozlov, V. V., and Ryzhov, O. S., 1990, "Receptivity of Boundary Layers: Asymptotic Theory and Experiment," *Proc. Roy. Soc. Lond.*, Vol. A-429, pp. 341-373.
- Lekoudis, S. G., Nayfeh, A. H., and Saric, W. S., 1976, "Compressible Boundary Layers Over Wavy Walls," *Phys. Fluids*, Vol. 19, No. 4, pp. 514-519.

Mack, L. M., 1984, "Boundary Layer Linear Stability Theory," In *Special Course on Stability and Transition of Laminar Flow*, AGARD Report 709.

Malik, M. R. and Orszag, S. A., 1987, "Linear Stability Analysis of Three-Dimensional, Compressible Boundary Layers," *J. of Sci. Comp.*, Vol. 2, pp. 77-97.

Masad J. and Nayfeh, A. H., 1992, "Laminar Flow Control of Subsonic Boundary Layers by Suction and Heat-Transfer Strips," *Phys. Fluids A*, Vol. 4, pp. 1259-1272.

Masad J. and Iyer, V., 1993, "Transition Prediction and Control in Subsonic Flow over a Hump," *Phys. Fluids A*, Vol. 6, No. 1, pp. 313-327.

Nishioka, M. and Morkovin, M. V., 1986, "Boundary Layer Receptivity to Unsteady Pressure Gradients: Experiments and Overview," *J. Fluid Mech.*, Vol. 171, pp. 219-261.

Reda, D. C., Reed, H. L., and Kobayashi, R., eds., 1991, "Boundary Layer Stability and Transition to Turbulence," FED-Vol. 114, ASME, NY.

Reed, H. L., and Nayfeh, A. H., 1985, "Numerical Perturbation Technique for Stability of Flat-Plate Boundary Layers with Suction," *AIAA J.*, Vol. 24, no. 2, pp. 208-214.

Reshotko, E., 1976, "Boundary Layer Stability and Transition," *Ann. Rev. Fluid Mech.*, Vol. 8, pp. 311-349.

Ruban, A. I., 1985, "On the Generation of Tollmien-Schlichting Waves by Sound," Transl. in *Fluid Dyn.*, Vol. 19, pp. 709-716.

Ryzhov, O. S., 1993, "An Asymptotic Approach to Separation and Stability Problems of a Transonic Boundary Layer," In *Transonic Aerodynamics: Problems in Asymptotic Theory*, SIAM, Philadelphia, pp. 29-53.

Ryzhov, O. S., and Zhuk, V. I., 1986, "On the Stability of a Compressible Boundary Layer against Three-Dimensional Disturbances with Self-Induced Pressure Gradient," Translation *Current Problems in Computational Fluid Dynamics*, Mir Publ., Moscow, pp. 286-307.

Ryzhov, O. S., and Savenkov, I. A., 1990, "Boundary Layer Stability in the Case of a Transonic Flow," *Zh. Prikl. Mekh. i Tekhn. Fiz.*, pp. 65-71.

Smith, F.T., 1989, "On the First Mode Instability in Subsonic, Supersonic, and Hypersonic Boundary Layers," *J. Fluid Mech.*, Vol. 198, pp. 127-153.

Stewartson, K., 1974, "Multistructured boundary layers on flat plates and related bodies," *Adv. Appl. Mech.*, Vol. 14, pp. 145-239.

Tam, C. K. W., 1981, "The Excitation of Tollmien-Schlichting Waves in Low Subsonic Boundary Layers by Free-Stream Sound Waves," *J. Fluid Mech.*, Vol. 109, pp. 483-501.

Tumin, A. M., and Fedorov, A. V., 1983, "Generation of Instability Waves in the Boundary Layers on Vibrating Surfaces," *Zh. Prikl. Mekh. i Tekhn. Fiz.*, pp. 72-79.

Zavol'skii, N. A., Reutov V. P. and Ryboushkina, G. V., 1983, "Generation of Tollmien-Schlichting Waves via Scattering of Acoustic and Vortex Perturbations in Boundary Layer on Wavy Surface," *Zh. Prikl. Mekh. i Tekhn. Fiz.*, pp. 79-86.

## Appendix

In this Appendix, we present the inhomogeneous set of equations that governs the unsteady scattered field  $\mathbf{Q}_{w,ac} \equiv (U_{w,ac}, V_{w,ac}, W_{w,ac}, T_{w,ac}, P_{w,ac})$ . Recall that the superscript ( $j$ ) in  $\mathbf{Q}_w^{(j)}$  and  $\mathbf{Q}_{w,ac}^{(j)}$  has been dropped for the simplicity of notation. As stated in section 2 of this paper, the above set of inhomogeneous equations can be expressed in the following form after a Fourier transform is taken in the streamwise and spanwise directions:

$$\mathbf{L}_{NS}(\alpha, \partial_Y, \beta, \omega, R_{\delta^*}) \bar{\mathbf{Q}}_{w,ac} = \mathbf{N}_{NS,2}(\bar{\mathbf{Q}}_w, \mathbf{Q}_{ac}), \quad (A1)$$

where the overbars denote the Fourier transforms of the perturbation quantities. The operator  $\mathbf{L}_{NS}$  on the left-hand side is the matrix form of the linear stability equations in the coordinate system ( $X, Y, Z$ ) that is introduced in Section 2. However, in the literature on the three-dimensional stability of quasi-parallel shear flows, it is customary to solve the relevant homogeneous equations in the wavefront (i.e., "Squire" coordinates) instead of solving them directly in the physical coordinate system. Hence, we will follow the same procedure here to solve the corresponding system of inhomogeneous equations. Thus, the  $X$ - and  $Z$ -momentum equations from the set (A1) will be replaced by the momentum equations along, and perpendicular to, the wavenumber vector  $(\alpha, \beta)$  in the

Fourier transform space. At the same time, the streamwise and spanwise velocities will be replaced as dependent variables by the horizontal divergence field  $\bar{q}_{w,ac}^+ \equiv \alpha \bar{U}_{w,ac} + \beta \bar{W}_{w,ac}$  and the field  $\bar{q}_{w,ac}^- \equiv \alpha \bar{W}_{w,ac} - \beta \bar{U}_{w,ac}$ , which is related to the vertical vorticity associated with the unsteady scattered field. After this transformation, the system of equations that corresponds to (A1) may be rewritten in the form

$$\tilde{\mathbf{L}}_{NS}(\alpha, \partial_Y, \beta, \omega, R_{\delta^*}) \tilde{\mathbf{Q}}_{w,ac} = \tilde{\mathbf{N}}_{NS;2}(\bar{\mathbf{Q}}_w, \mathbf{Q}_{ac}), \quad (\text{A2})$$

where the new array of dependent variables  $\tilde{\mathbf{Q}}_{w,ac}$  corresponds to  $(\bar{q}_{w,ac}^+, \bar{V}_{w,ac}, \bar{q}_{w,ac}^-, \bar{T}_{w,ac}, \bar{P}_{w,ac})$ . The operator  $\tilde{\mathbf{L}}_{NS}$  represents the linear stability equations in the rotated (i.e., Squire) coordinate system and has the form

$$\tilde{\mathbf{L}}_{NS} = \mathbf{A} \frac{d^2}{dY^2} + \mathbf{B} \frac{d}{dY} + \mathbf{C}, \quad (\text{A3})$$

where the coefficient matrices  $\mathbf{A}$ ,  $\mathbf{B}$ , and  $\mathbf{C}$  can be obtained from the expressions given in Malik and Orszag (1987) and, therefore, will not be repeated in this paper.

The forcing vector  $\tilde{\mathbf{N}}_{NS;2}$  in (A2) can be expressed in the form

$$\tilde{\mathbf{N}}_{NS;2} = \tilde{\mathbf{N}}_{inv;2} + \tilde{\mathbf{N}}_{visc;2}, \quad (\text{A4})$$

where the vectors  $\tilde{\mathbf{N}}_{inv;2}$  and  $\tilde{\mathbf{N}}_{visc;2}$  represent the bilinear interaction terms that arise from the inviscid and viscous terms, respectively, in the Navier-Stokes equations. The coefficients of the viscous source terms in the momentum and the energy equations are smaller than those of the corresponding inviscid terms by a factor of  $O(R_{\delta^*})$ . Hence, the error incurred in the prediction of the instability-wave amplitude by neglecting the viscous terms from the forcing  $\tilde{\mathbf{N}}_{NS;2}$  would appear to be  $O(1/R_{\delta^*})$ , or of the same order as the error in neglecting the effects of base-flow variation (i.e., growth of the mean boundary layer) across the region of nonuniformity. However, this conjecture is incorrect because some of the “ $O(1/R_{\delta^*})$ ” terms involve first or second derivatives of the mean-flow disturbance and/or the acoustic-signature field with respect to  $Y$ , which can become rather large in certain localized regions across the boundary layer. Thus, the contribution from these terms (relative to that of the inviscid nonlinearities) is actually larger than  $O(1/R_{\delta^*})$ . The precise order of the contribution from each term of this type can only be determined after we have considered all asymptotic subregions that characterize the mean-flow

disturbance, the acoustic-signature field, and the instability wave. Nevertheless, the magnitude of the contribution from each viscous term is already related to the corresponding sum of the orders of derivatives of the first-order perturbations  $\bar{\mathbf{Q}}_w$  and  $\mathbf{Q}_{ac}$  with respect to the wall-normal coordinate.

The set of viscous forcing terms may then be further classified as

$$\tilde{\mathbf{N}}_{visc;2} = \tilde{\mathbf{N}}_{visc;2}^{(2)} + \tilde{\mathbf{N}}_{visc;2}^{(1)} + \tilde{\mathbf{N}}_{visc;2}^{(0)}, \quad (\text{A5})$$

where the superscripts within parentheses on the right-hand side of (A5) indicate the sum of the orders of derivatives of  $\bar{\mathbf{Q}}_w$  and  $\mathbf{Q}_{ac}$  with respect to  $Y$ . A larger value of the superscript indicates that the overall contribution from that subclass of viscous terms is more dominant. Thus, terms that belong to  $\tilde{\mathbf{N}}_{visc;2}^{(2)}$  provide the largest viscous contribution, as a whole, to the amplitude of the generated instability wave. These terms can become comparable to the inviscid forcing terms in certain localized regions of the boundary layer, such as the viscous layer close to the wall. However, as we mentioned previously, in the absence of a rigorous asymptotic analysis, decision as to whether the overall contribution from these terms is comparable to that of the inviscid forcing (or whether it simply provides the dominant correction for the latter) is difficult. In either case, terms from  $\tilde{\mathbf{N}}_{visc;2}^{(1)}$  provide a higher order correction, which is larger than  $O(1/R_{\delta^*})$ . On the other hand, the terms in  $\tilde{\mathbf{N}}_{visc;2}^{(0)}$  are uniformly of  $O(1/R_{\delta^*})$  with respect to the inviscid terms; therefore, these terms may be safely neglected on the grounds stated in the previous paragraph. The only reason for including them in the numerical calculation would be to maintain consistency with the adopted framework of the quasi-parallel stability theory.

The overall contribution from  $\tilde{\mathbf{N}}_{visc;2}^{(1)}$  and  $\tilde{\mathbf{N}}_{visc;2}^{(0)}$  was small, even at Mach numbers as large as 4.5. The numerical results presented in this paper include the effects of both source terms; however, because the expressions for these terms are rather lengthy, we have omitted them from this appendix. Thus, only the expressions for the inviscid forcing terms  $\tilde{\mathbf{N}}_{inv;2}$  and the dominant viscous terms  $\tilde{\mathbf{N}}_{visc;2}^{(2)}$  are given below. The first three elements of each of these vectors correspond to the source terms in the momentum equations that correspond to  $\bar{q}_{w,ac}^+$ ,  $\bar{V}_{w,ac}$  and  $\bar{q}_{w,ac}^-$ , respectively; the fourth and fifth elements correspond to the forcing in the energy and continuity equations, respectively. In deriving the expressions for these

source terms, we have assumed that the specific heat  $C_{p\infty}^*$ , the ratio of specific heats  $\gamma$ , and the Prandtl number  $\sigma$  are all constant quantities. In addition, the Stokes hypothesis has been assumed to be valid. The primes in these equations denote derivatives with respect to the wall-normal coordinate  $Y$ . Because of the lengthy nature of the expressions involved, the latter have also been checked with the symbolic manipulation package *Mathematica*. Expressions for  $\tilde{\mathbf{N}}_{visc;2}^{(1)}$  and  $\tilde{\mathbf{N}}_{visc;2}^{(0)}$  are available from the author upon request.

$$\begin{aligned}\tilde{\mathbf{N}}_{inv;2}(1) &= \frac{R_{\delta^*}}{\mu_0} \left\{ -i\omega\bar{\rho}_w(\alpha U_{ac} + \beta W_{ac}) \right. \\ &+ \frac{1}{T_0} [i(\alpha_{ac}\bar{U}_w + \beta_{ac}\bar{W}_w)(\alpha U_{ac} + \beta W_{ac}) \\ &\quad + \bar{V}_w(\alpha U'_{ac} + \beta W'_{ac}) \\ &\quad + i(\alpha_w U_{ac} + \beta_w W_{ac})(\alpha\bar{U}_w + \beta\bar{W}_w) \\ &\quad + V_{ac}(\alpha\bar{U}'_w + \beta\bar{W}'_w)] \\ &+ \bar{\rho}_w [i(\alpha_{ac}U_0 + \beta_{ac}W_0)(\alpha U_{ac} + \beta W_{ac}) \\ &\quad + V_{ac}(\alpha U'_0 + \beta W'_0)] \\ &+ \rho_{ac} [i(\alpha_w U_0 + \beta_w W_0)(\alpha\bar{U}_w + \beta\bar{W}_w) \\ &\quad \left. + \bar{V}_w(\alpha U'_0 + \beta W'_0)] \right\}\end{aligned}$$

$$\begin{aligned}\tilde{\mathbf{N}}_{inv;2}(2) &= \frac{3}{4} \frac{R_{\delta^*}}{\mu_0} \left\{ -i\omega\bar{\rho}_w V_{ac} \right. \\ &+ \frac{1}{T_0} [i(\alpha_{ac}\bar{U}_w + \beta_{ac}\bar{W}_w)V_{ac} + \bar{V}_w V'_{ac} \\ &\quad + i(\alpha_w U_{ac} + \beta_w W_{ac})\bar{V}_w + V_{ac}\bar{V}'_w] \\ &\quad + i\bar{\rho}_w(\alpha_{ac}U_0 + \beta_{ac}W_0)V_{ac} \\ &\quad \left. + i\rho_{ac}(\alpha_w U_0 + \beta_w W_0)\bar{V}_w \right\}\end{aligned}$$

$$\begin{aligned}\tilde{\mathbf{N}}_{inv;2}(3) &= \frac{R_{\delta^*}}{\mu_0} \left\{ -i\omega\bar{\rho}_w(-\beta U_{ac} + \alpha W_{ac}) \right. \\ &+ \frac{1}{T_0} [i(\alpha_{ac}\bar{U}_w + \beta_{ac}\bar{W}_w)(-\beta U_{ac} + \alpha W_{ac}) \\ &\quad + \bar{V}_w(-\beta U'_{ac} + \alpha W'_{ac}) \\ &\quad \left. + i(\alpha_w U_{ac} + \beta_w W_{ac})(-\beta\bar{U}_w + \alpha\bar{W}_w) \right\}\end{aligned}$$

$$\begin{aligned}&+ V_{ac}(-\beta\bar{U}'_w + \alpha\bar{W}'_w)] \\ &+ \bar{\rho}_w [i(\alpha_{ac}U_0 + \beta_{ac}W_0)(-\beta U_{ac} + \alpha W_{ac}) \\ &\quad + V_{ac}(-\beta U'_0 + \alpha W'_0)] \\ &+ \rho_{ac} [i(\alpha_w U_0 + \beta_w W_0)(-\beta\bar{U}_w + \alpha\bar{W}_w) \\ &\quad + \bar{V}_w(-\beta U'_0 + \alpha W'_0)] \left. \right\}\end{aligned}$$

$$\begin{aligned}\tilde{\mathbf{N}}_{inv;2}(4) &= \frac{\sigma R_{\delta^*}}{\mu_0} \left\{ -i\omega\bar{\rho}_w T_{ac} \right. \\ &+ \frac{1}{T_0} [i(\alpha_{ac}\bar{U}_w + \beta_{ac}\bar{W}_w)T_{ac} + \bar{V}_w T'_{ac} \\ &\quad + i(\alpha_w U_{ac} + \beta_w W_{ac})\bar{T}_w + V_{ac}\bar{T}'_w] \\ &+ \bar{\rho}_w [i(\alpha_{ac}U_0 + \beta_{ac}W_0)T_{ac} + V_{ac}T'_0] \\ &\quad + \rho_{ac} [i(\alpha_w U_0 + \beta_w W_0)\bar{T}_w + \bar{V}_w T'_0] \\ &\quad - (\gamma - 1)M_\infty^2 [i(\alpha_{ac}\bar{U}_w + \beta_{ac}\bar{W}_w)P_{ac} + \bar{V}_w P'_{ac} \\ &\quad \left. + i(\alpha_w U_{ac} + \beta_w W_{ac})\bar{P}_w + V_{ac}\bar{P}'_w] \right\}\end{aligned}$$

$$\begin{aligned}\tilde{\mathbf{N}}_{inv;2}(5) &= -T_0 \left\{ i(\alpha_{ac}\bar{U}_w + \beta_{ac}\bar{W}_w)\rho_{ac} + \rho'_{ac}\bar{V}_w \right. \\ &\quad + i(\alpha_w U_{ac} + \beta_w W_{ac})\bar{\rho}_w + V_{ac}\bar{\rho}'_w \\ &\quad + \bar{\rho}_w [i(\alpha_{ac}U_{ac} + \beta_{ac}W_{ac}) + V'_{ac}] \\ &\quad \left. + \rho_{ac} [i(\alpha_w\bar{U}_w + \beta_w\bar{W}_w) + \bar{V}'_w] \right\} \\ &+ i((\alpha U_0 + \beta W_0) - \omega)(\bar{\rho}_w T_{ac} + \rho_{ac}\bar{T}_w)\end{aligned}$$

$$\begin{aligned}\tilde{\mathbf{N}}_{visc;2}^{(2)}(1) &= -\frac{1}{\mu_0} \frac{d\mu}{dT_0} [\bar{T}_w(\alpha U''_{ac} + \beta W''_{ac}) \\ &\quad + T_{ac}(\alpha\bar{U}''_w + \beta\bar{W}''_w) \\ &\quad + \bar{T}'_w(\alpha U'_{ac} + \beta W'_{ac}) + T'_{ac}(\alpha\bar{U}'_w + \beta\bar{W}'_w)]\end{aligned}$$

$$\tilde{\mathbf{N}}_{visc;2}^{(2)}(2) = -\frac{1}{\mu_0} \frac{d\mu}{dT_0} [\bar{T}_w V''_{ac} + T_{ac}\bar{V}''_w + \bar{T}'_w V'_{ac} + T'_{ac}\bar{V}'_w]$$

$$\begin{aligned}\tilde{\mathbf{N}}_{visc;2}^{(2)}(3) &= -\frac{1}{\mu_0} \frac{d\mu}{dT_0} [\bar{T}_w(-\beta U''_{ac} + \alpha W''_{ac}) \\ &\quad + T_{ac}(-\beta\bar{U}''_w + \alpha\bar{W}''_w) \\ &\quad + \bar{T}'_w(-\beta U'_{ac} + \alpha W'_{ac}) + T'_{ac}(-\beta\bar{U}'_w + \alpha\bar{W}'_w)]\end{aligned}$$

$$\begin{aligned}\tilde{\mathbf{N}}_{visc;2}^{(2)}(4) &= -\frac{1}{\mu_0} \frac{d\mu}{dT_0} (\bar{T}_w T''_{ac} + T_{ac}\bar{T}''_w + \bar{T}'_w T'_{ac} + T'_{ac}\bar{T}'_w) \\ &\quad - 2\sigma(\gamma - 1)M_\infty^2 \left( \bar{U}'_w U'_{ac} + \bar{W}'_w W'_{ac} + \frac{4}{3}\bar{V}'_w V'_{ac} \right)\end{aligned}$$

$$\tilde{\mathbf{N}}_{visc;2}^{(2)}(5) = 0$$

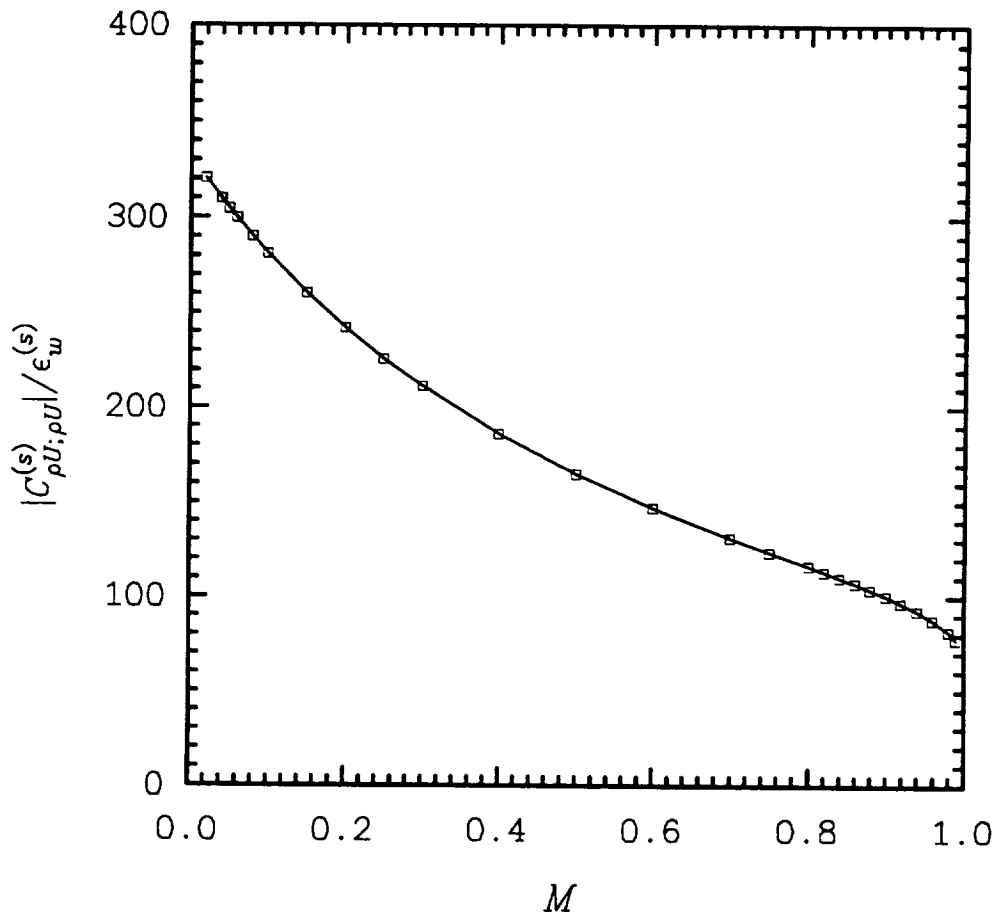


Figure 1(a). Influence of Mach number on magnitude of  $|C_{\rho U; \rho U}^{(s)}| / \epsilon_w^{(s)}$  with  $T_{sign} = 311$  K,  $R = \sqrt{Re_2} = 955$ ,  $\omega = \omega_{lb}$ ,  $\beta_{ins} = 0$ , and  $\theta_{ac} = 45^\circ$ .

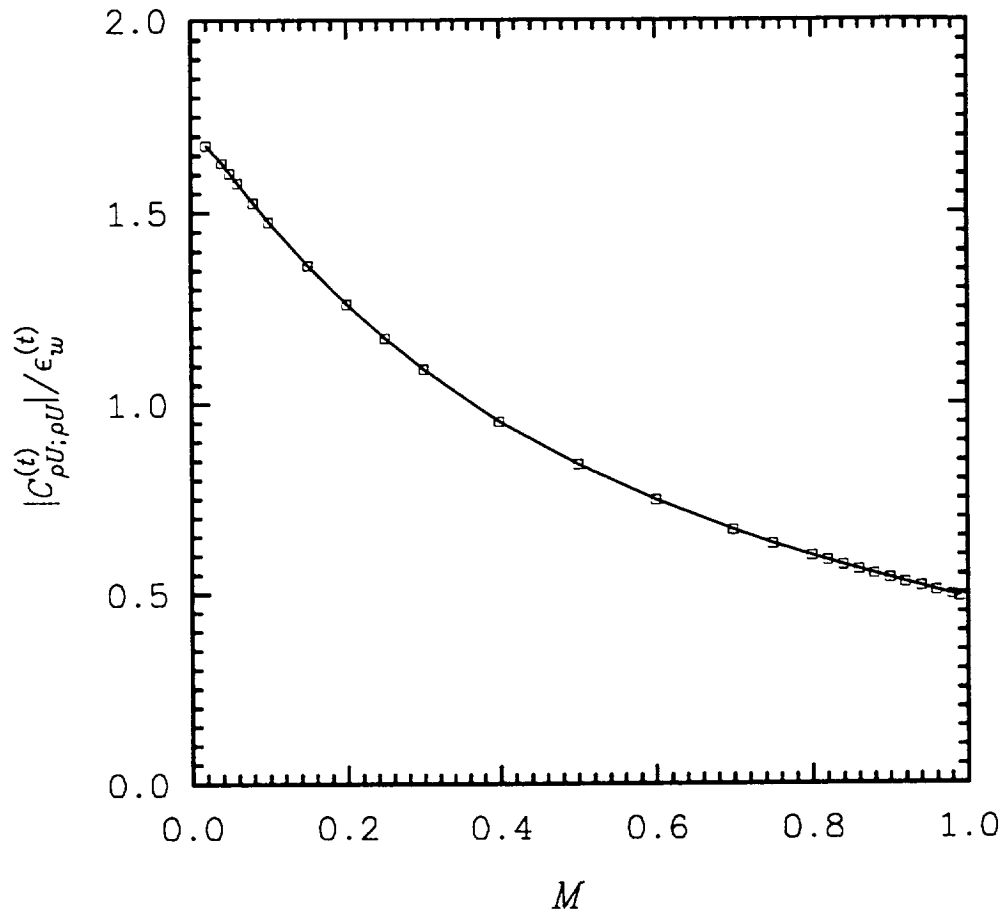


Figure 1(b). Influence of Mach number on magnitude of  $|C_{\rho U; \rho U}^{(t)}| / \epsilon_w^{(t)}$  with  $T_{stgn} = 311$  K,  $R = \sqrt{Re_2} = 955$ ,  $\omega = \omega_{1b}$ ,  $\beta_{ins} = 0$ , and  $\theta_{ac} = 45^\circ$ .

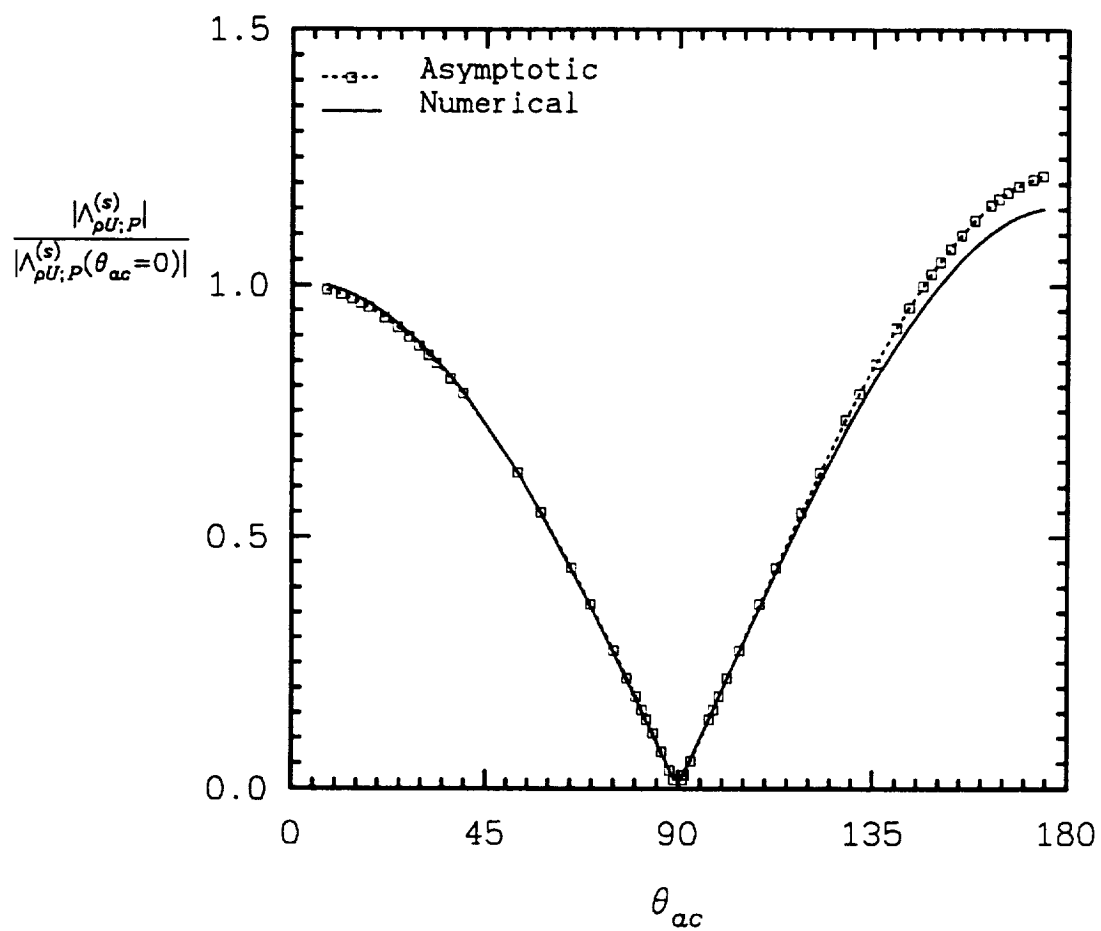


Figure 2(a). Influence of acoustic-wave orientation on  $|\Lambda_{\rho U; P}^{(s)}|$  with  $M = 0.1$ ,  $T_{stgn} = 311$  K,  $R = \sqrt{Re_2} = 955$ ,  $\omega \approx \omega_{1b}$ , and  $\beta_{ins} = 0.0$ .

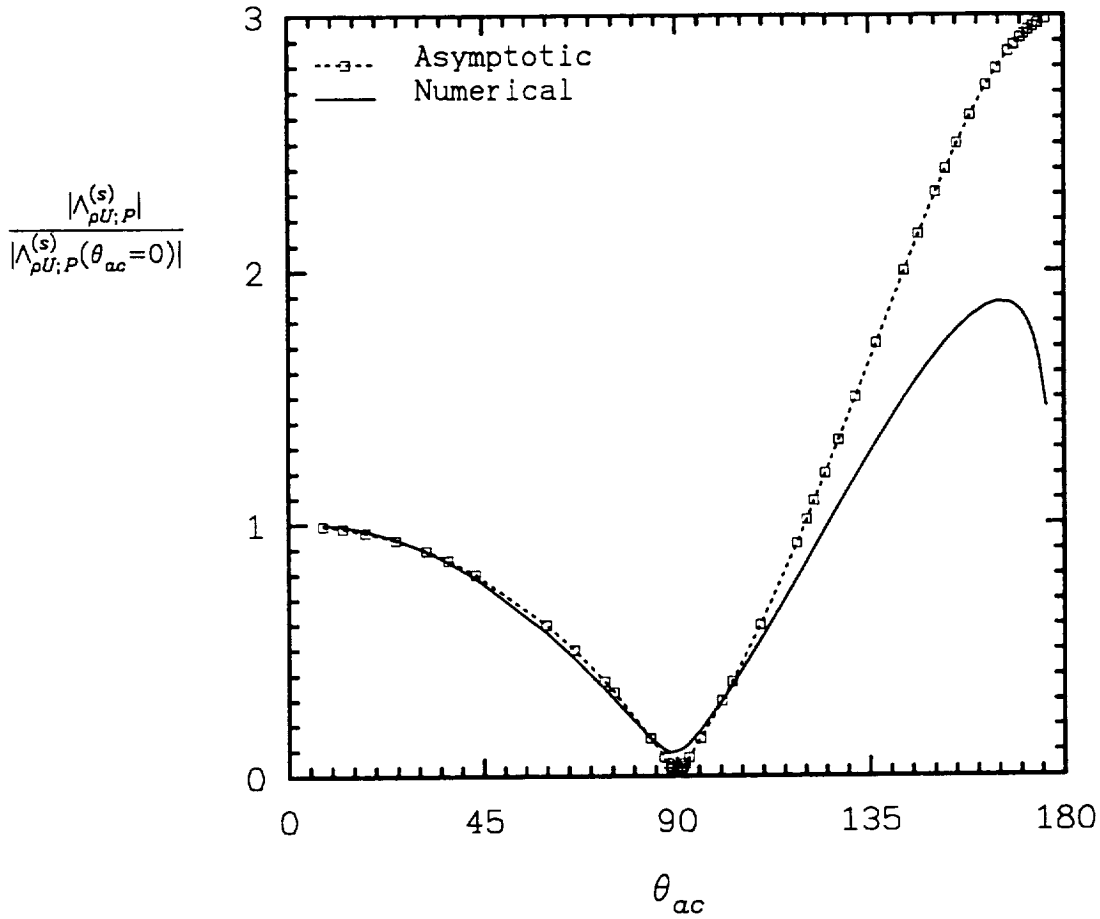


Figure 2(b). Influence of acoustic-wave orientation on  $|\Lambda_{\rho U;P}^{(s)}|$  with  $M = 0.5$ ,  $T_{stgn} = 311$  K,  $R = \sqrt{Re_2} = 955$ ,  $\omega \approx \omega_{lb}$ , and  $\beta_{ins} = 0.0$ .

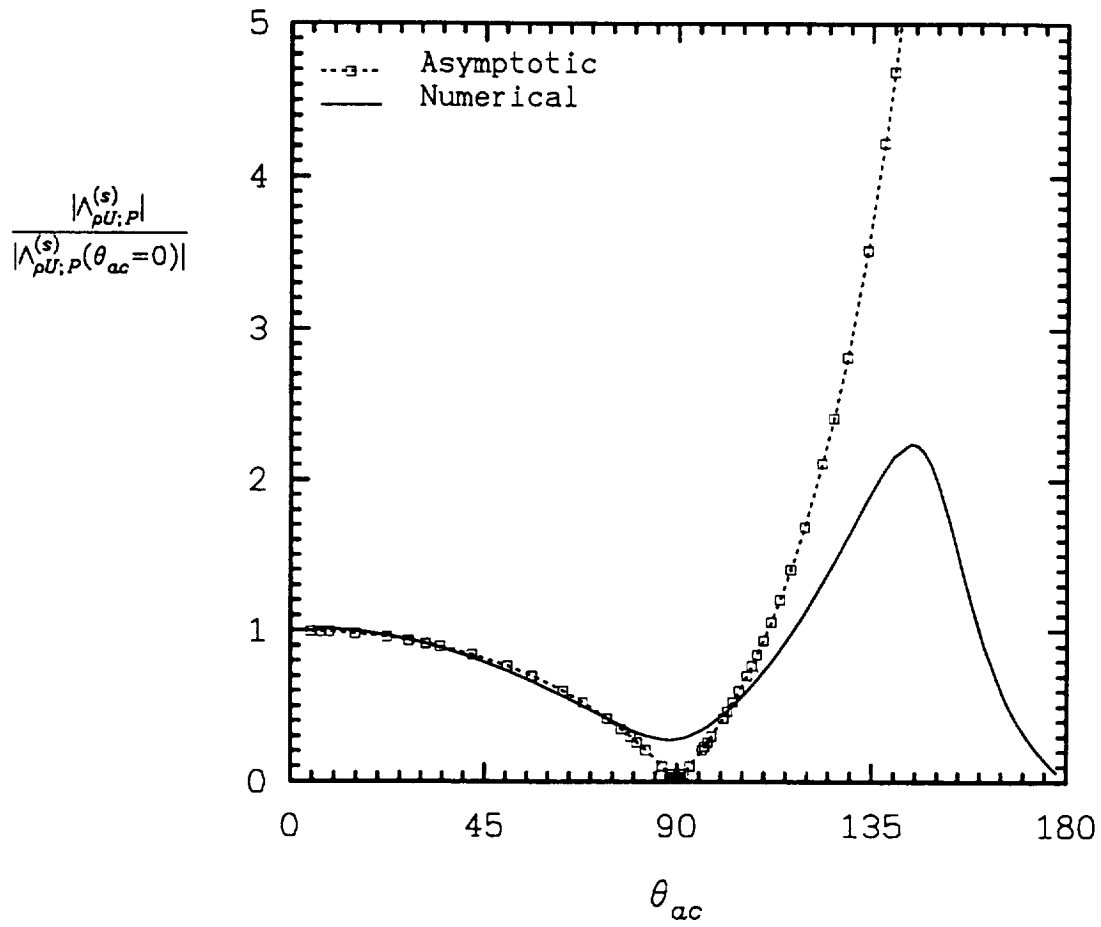


Figure 2(c). Influence of acoustic-wave orientation on  $|\Lambda_{\rho U;P}^{(s)}|$  with  $M = 0.9$ ,  $T_{stgn} = 311$  K,  $R = \sqrt{Re_2} = 955$ ,  $\omega \approx \omega_{lb}$ , and  $\beta_{ins} = 0.0$ .

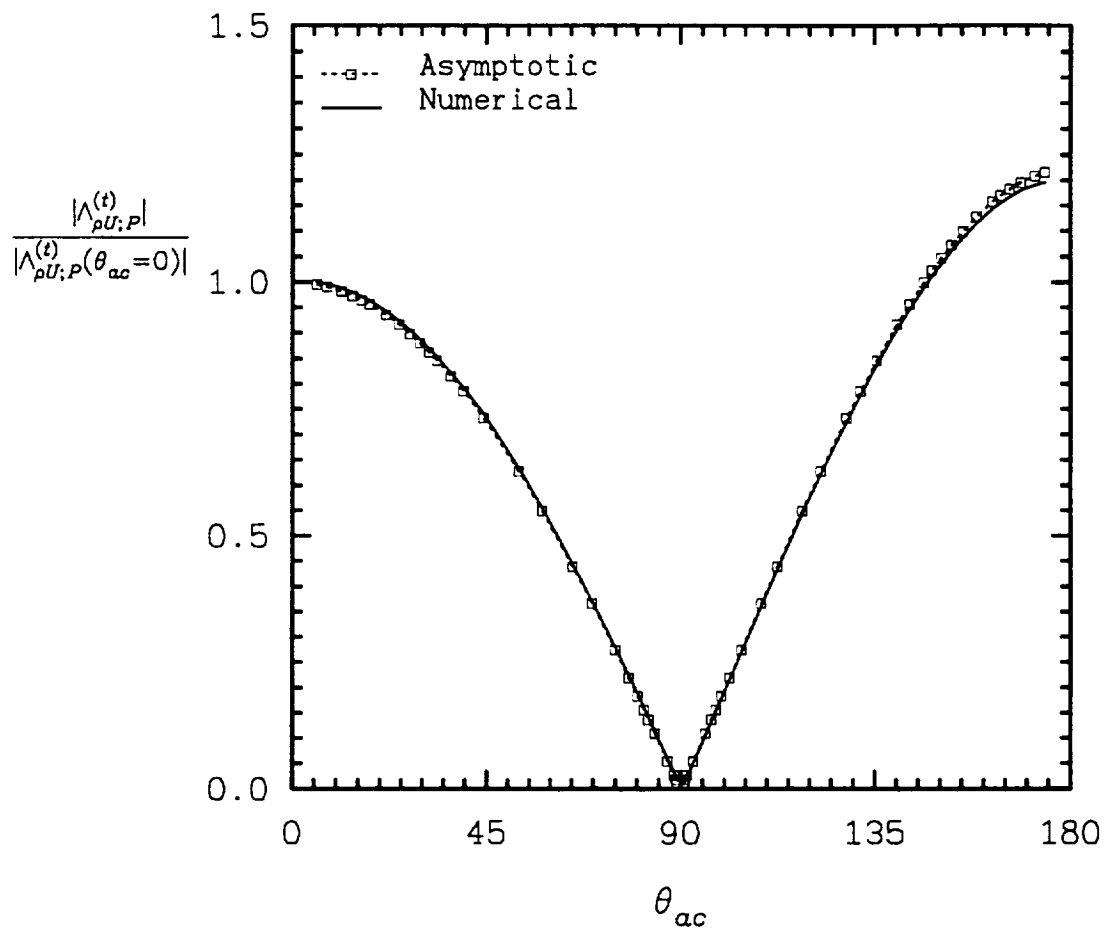


Figure 3(a). Influence of acoustic-wave orientation on  $|\Lambda_{\rho U;P}^{(t)}|$  with  $M = 0.1$ ,  $T_{stgn} = 311$  K,  $R = \sqrt{Re_2} = 955$ ,  $\omega \approx \omega_{1b}$ , and  $\beta_{ins} = 0.0$ .

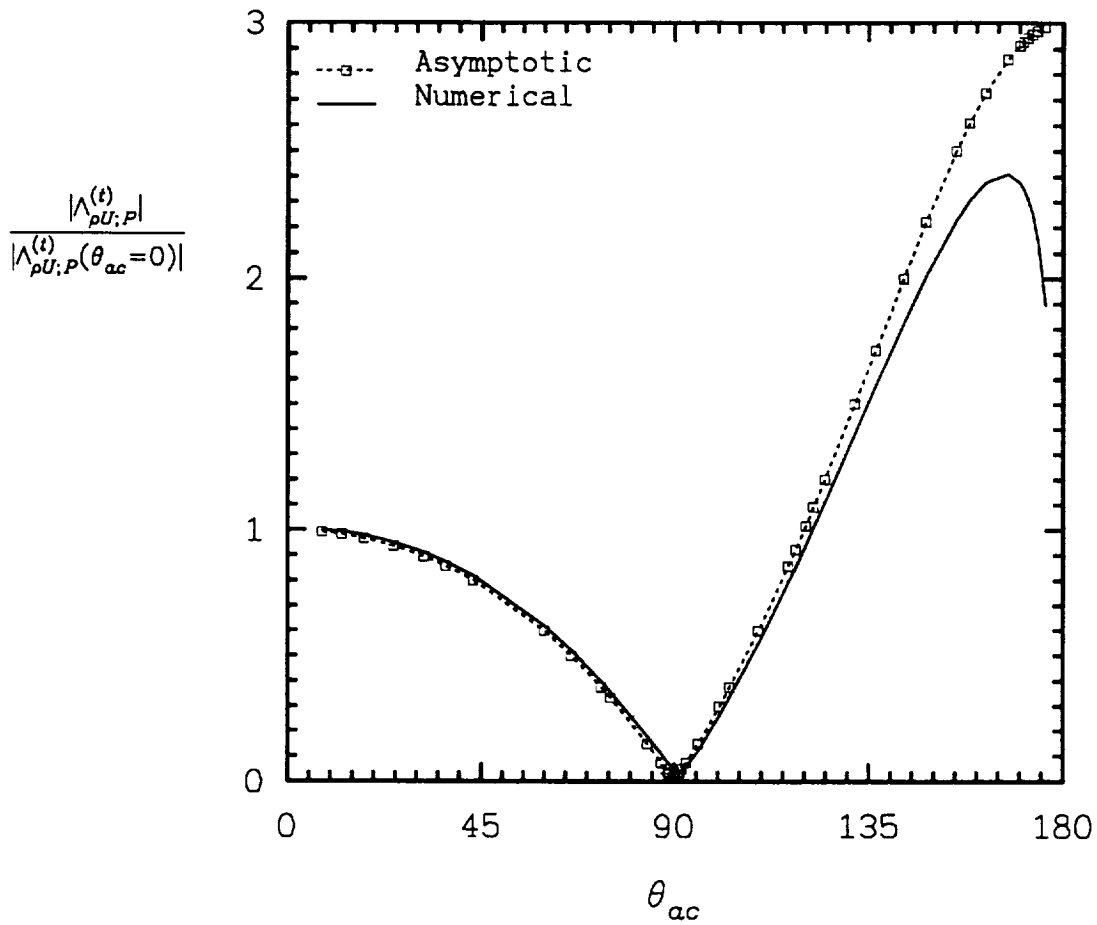


Figure 3(b). Influence of acoustic-wave orientation on  $|\Lambda_{\rho U; P}^{(t)}|$  with  $M = 0.5$ ,  $T_{stgn} = 311$  K,  $R = \sqrt{Re_2} = 955$ ,  $\omega \approx \omega_{1b}$ , and  $\beta_{ins} = 0.0$ .

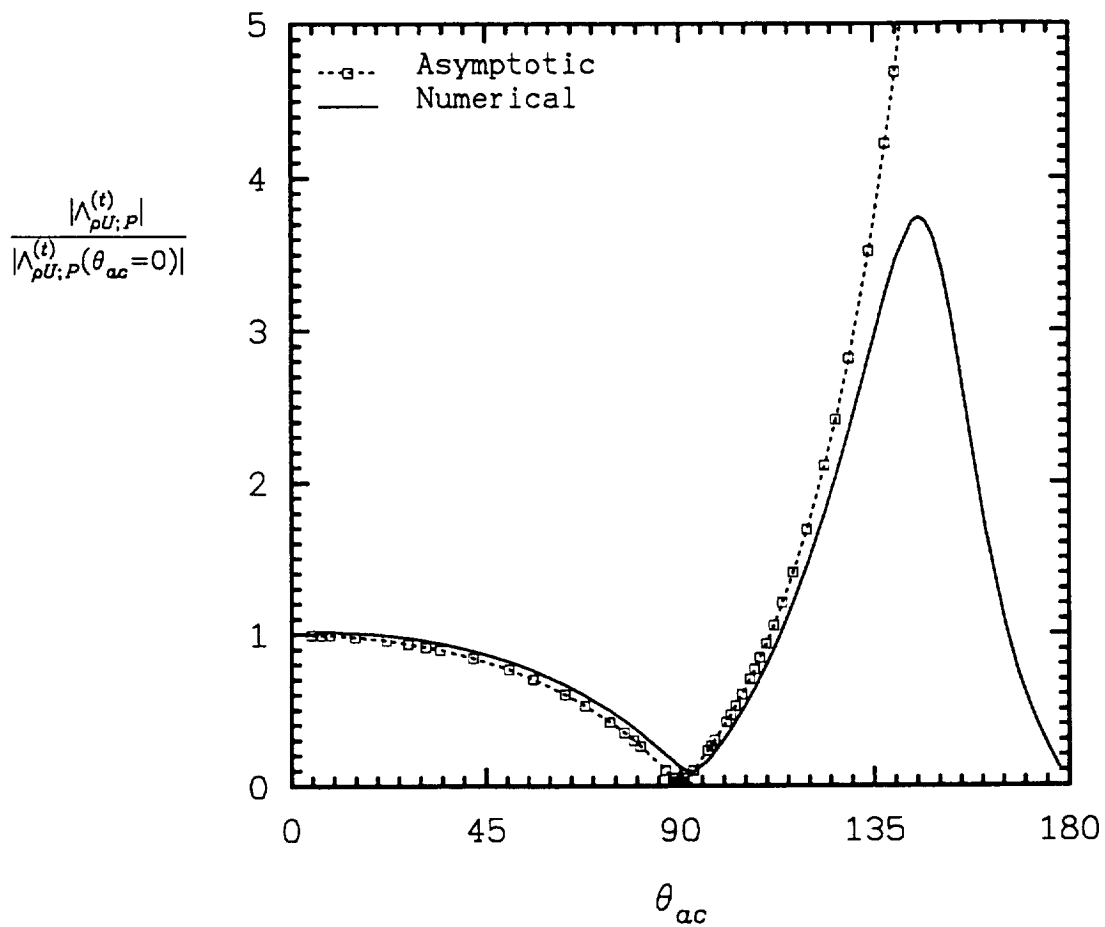


Figure 3(c). Influence of acoustic-wave orientation on  $|\Lambda_{\rho U; P}^{(t)}|$  with  $M = 0.9$ ,  $T_{stgn} = 311$  K,  $R = \sqrt{Re_2} = 955$ ,  $\omega \approx \omega_{lb}$ , and  $\beta_{tns} = 0.0$ .

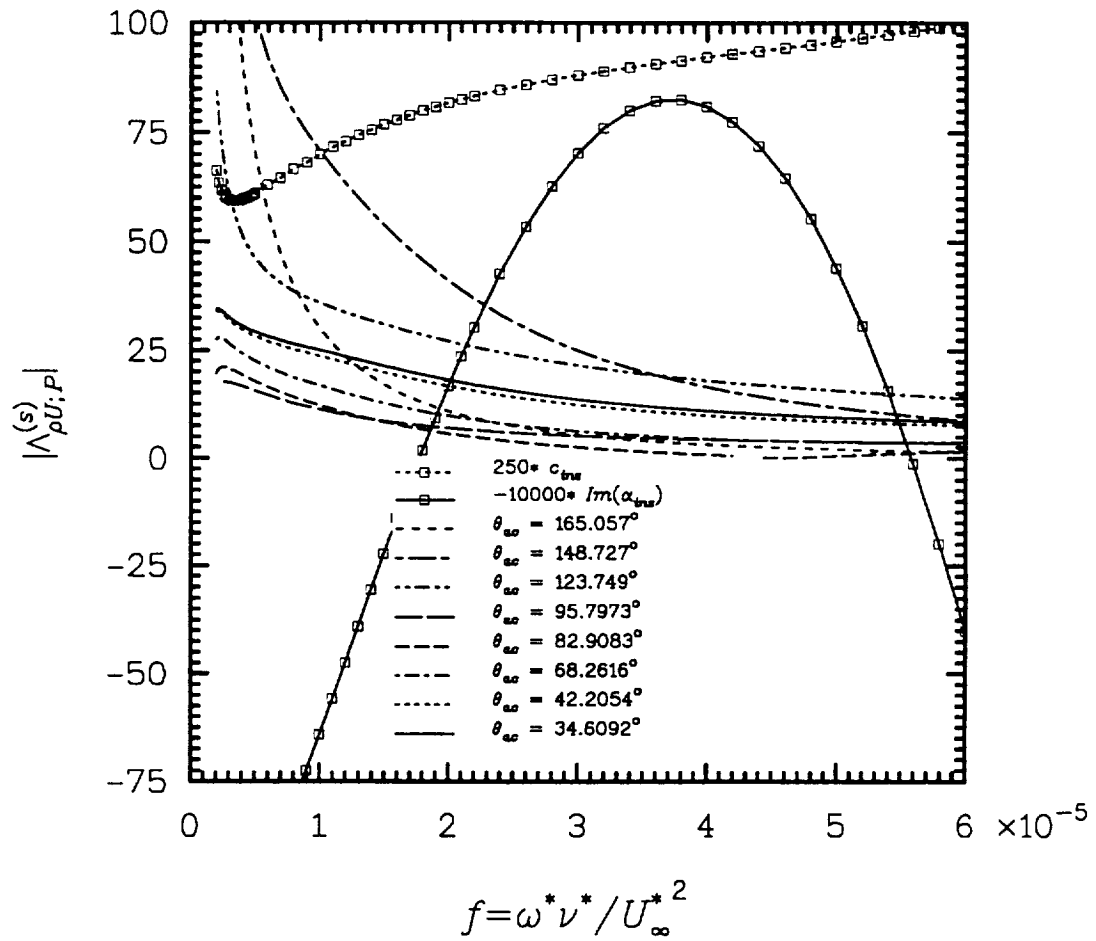


Fig. 4(a). Variation of  $|\Lambda_{\rho U;P}^{(s)}|$  with  $f$  at fixed strip location with  $T_{stgn} = 311$  K,  $R = \sqrt{Re_L} = 955$ , and  $\beta_{trns} = 0$ .

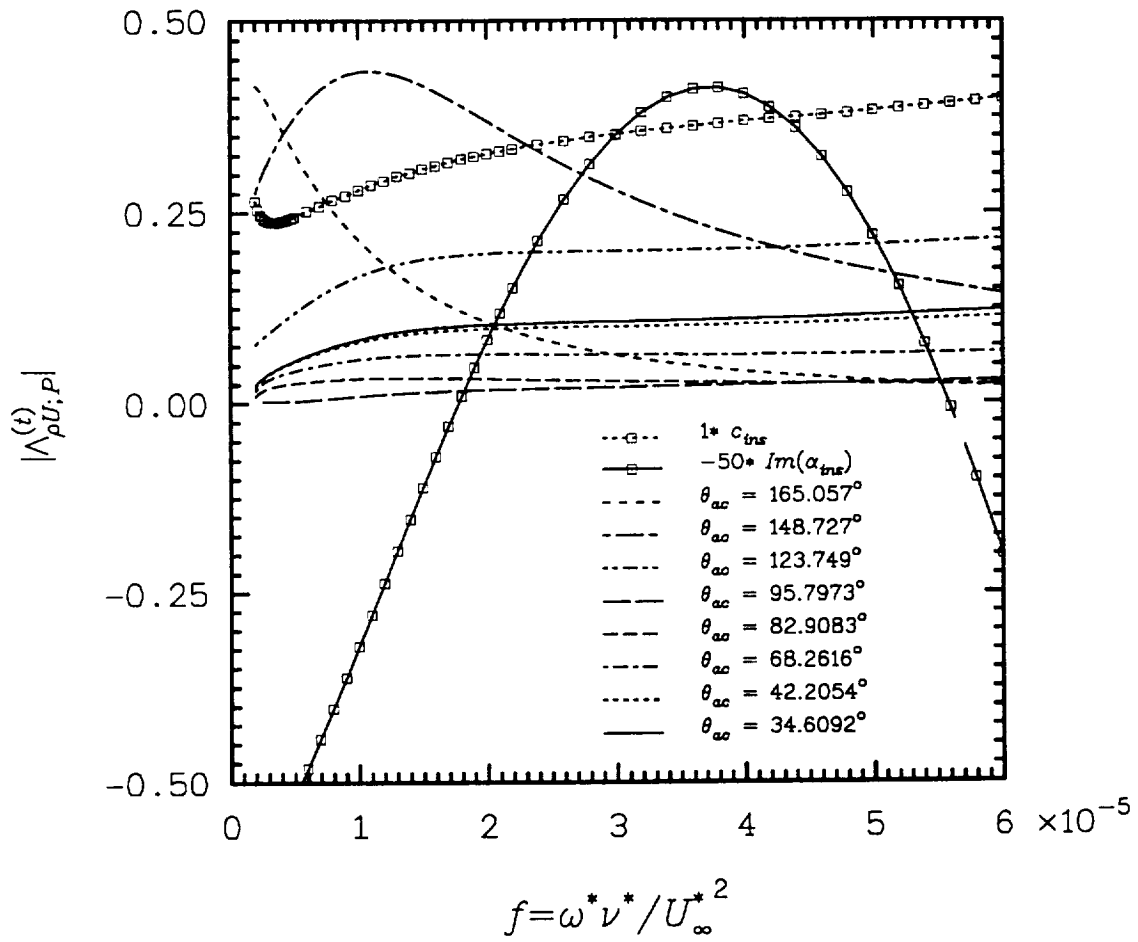


Fig. 4(b). Variation of  $|\Lambda_{\rho U; P}^{(t)}|$  with  $f$  at fixed strip location with  $T_{stgn} = 311$  K,  $R = \sqrt{Re_l} = 955$ , and  $\beta_{ins} = 0$ .

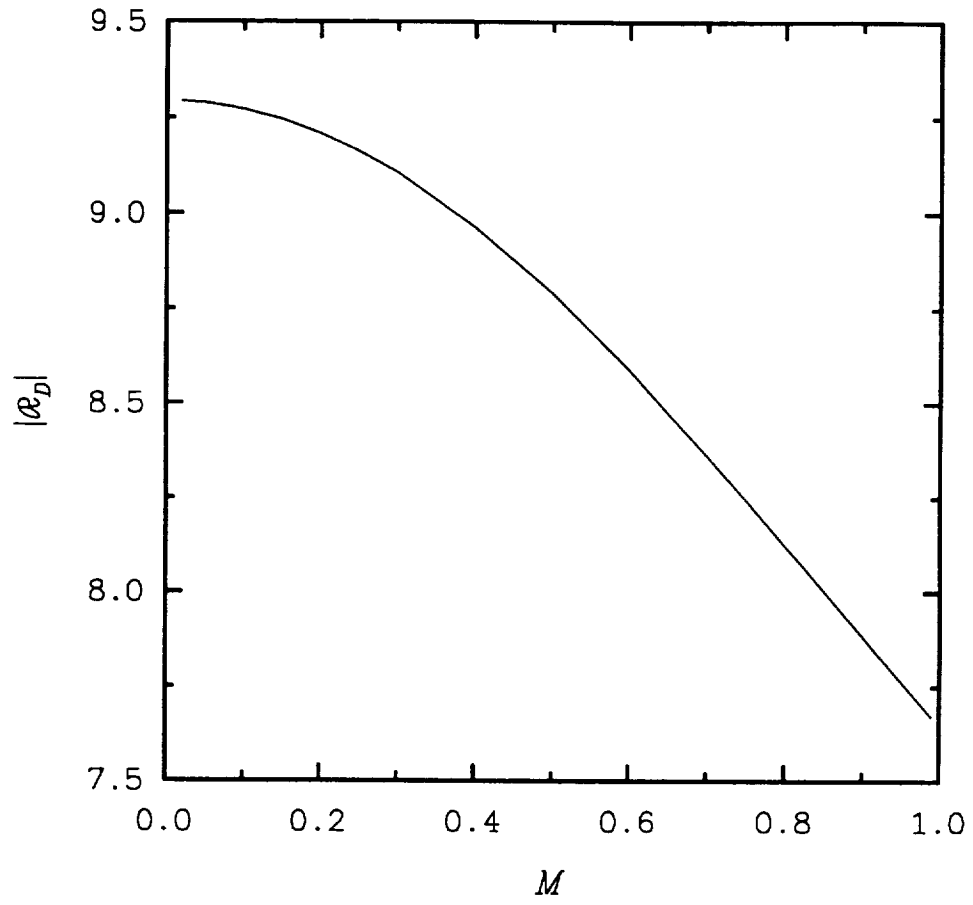


Figure 5. Magnitude of factor  $\rho_D$  from (9d) as function of  $M$ .

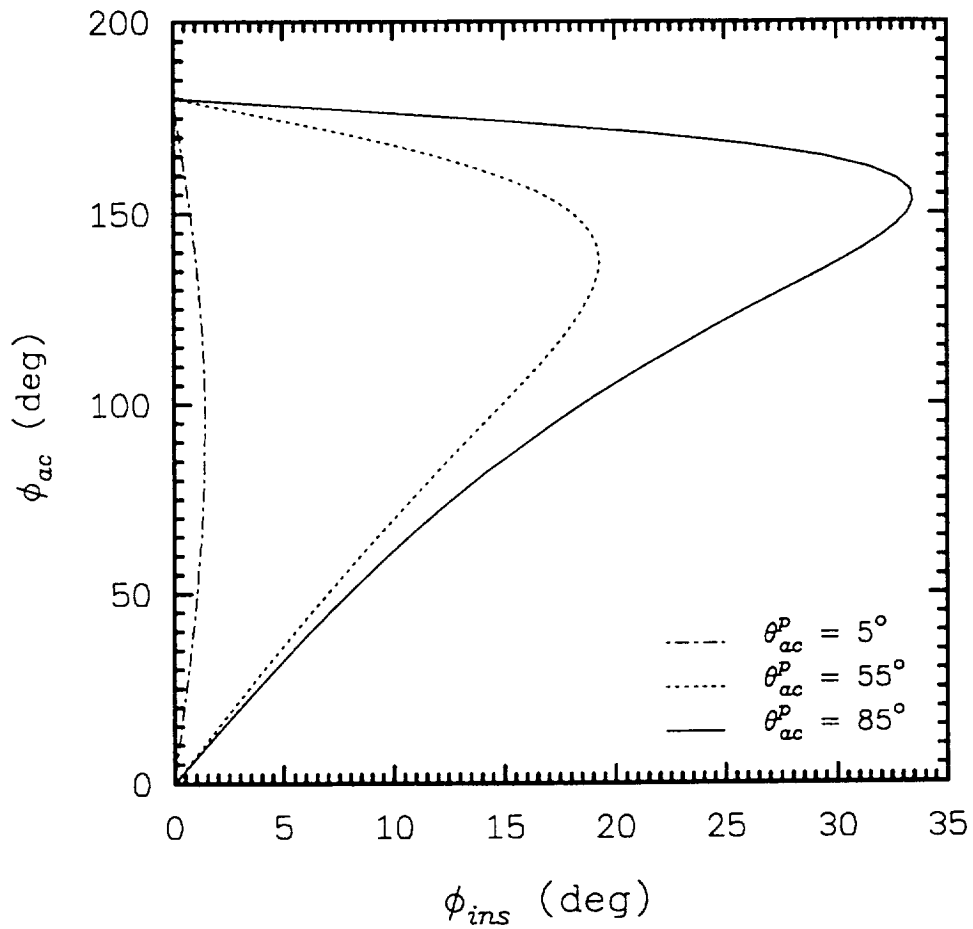


Figure 6(a). Excitation of three-dimensional instability waves near two-dimensional nonuniformity :  $\phi_{ac}$  (deg) is plotted against  $\phi_{ins}$  (deg) with  $M = 0.9$ ,  $T_{stgn} = 311$  K,  $R \equiv \sqrt{Re_\ell} = 955$ , and  $f \equiv \omega/R_\delta = 18E-06$ .

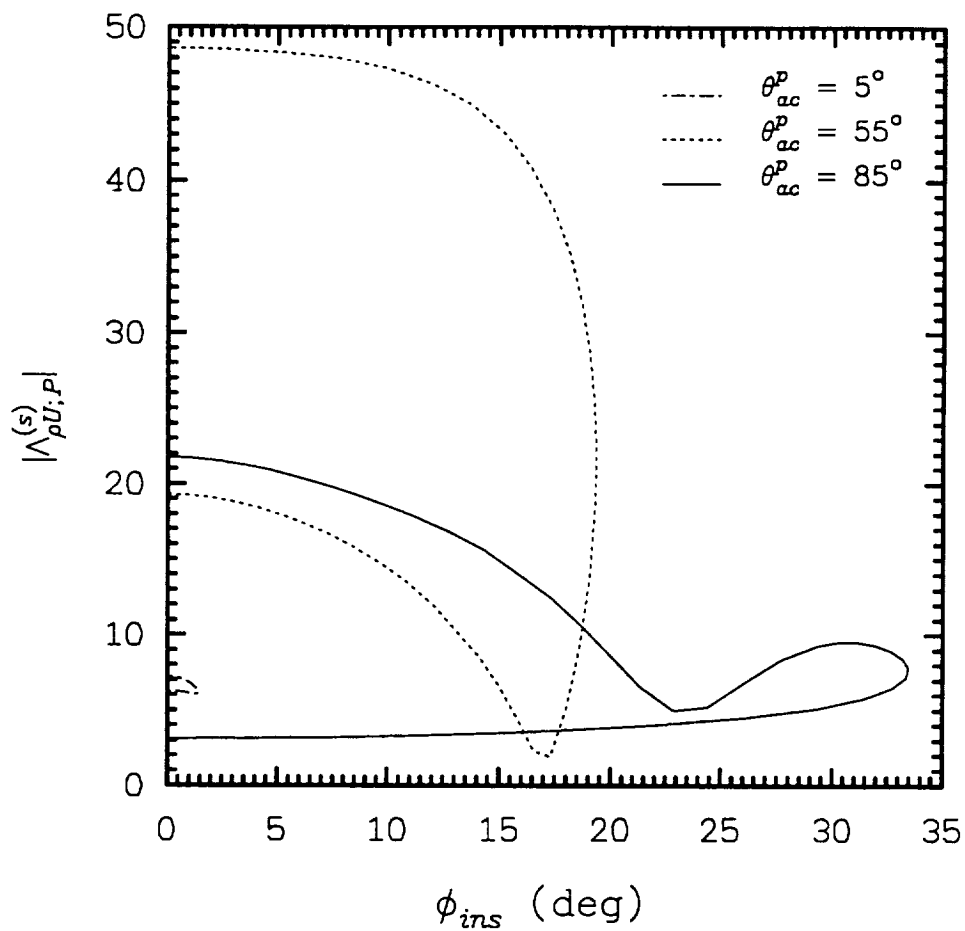


Figure 6(b). Excitation of three-dimensional instability waves near two-dimensional suction strip:  $|\Lambda_{\rho U;P}^{(s)}|$  is plotted against  $\phi_{ins}$  (deg) with  $M = 0.9$ ,  $T_{stgn} = 311$  K,  $R \equiv \sqrt{Re_2} = 955$ , and  $f \equiv \omega/R_g = 18E-06$ .

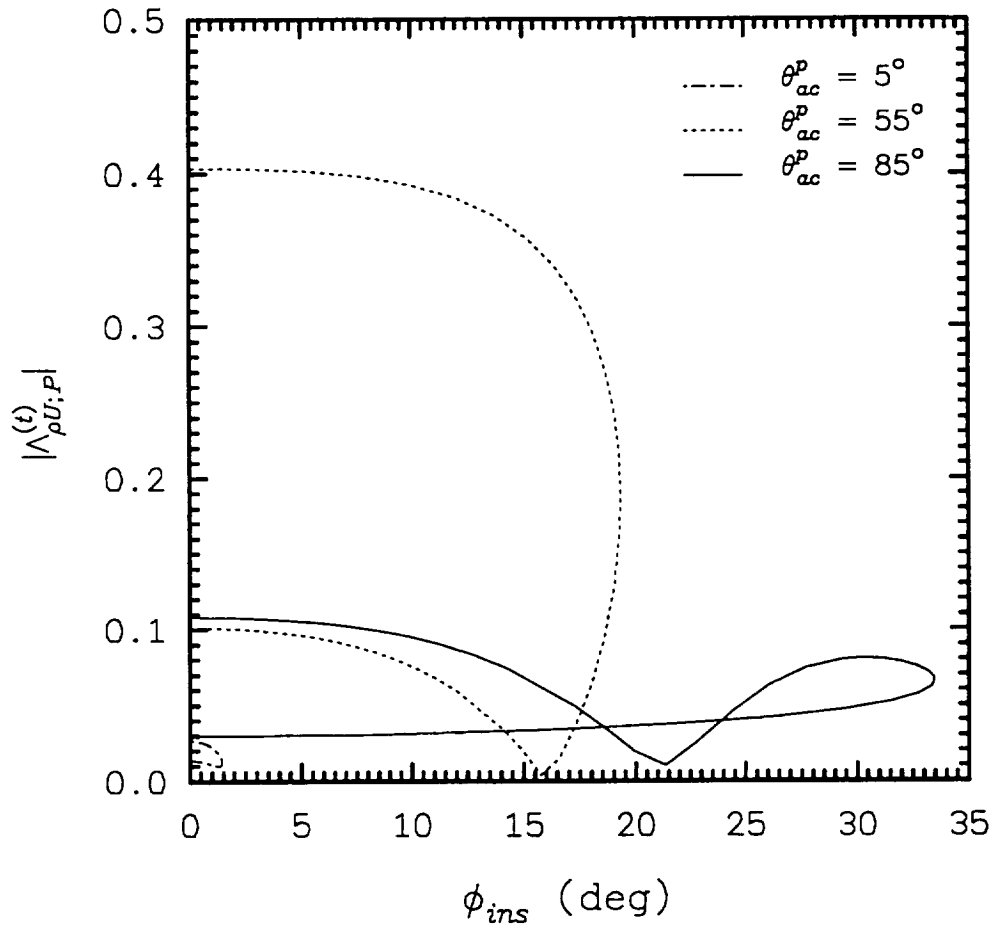


Figure 6(c). Excitation of three-dimensional instability waves near two-dimensional heat-transfer strip:  $|\Lambda_{\rho U;P}^{(t)}|$  is plotted against  $\phi_{ins}$  (deg) with  $M = 0.9$ ,  $T_{stgn} = 311$  K,  $R \equiv \sqrt{Re_2} = 955$ , and  $f \equiv \omega/R_\delta = 18E-06$ .

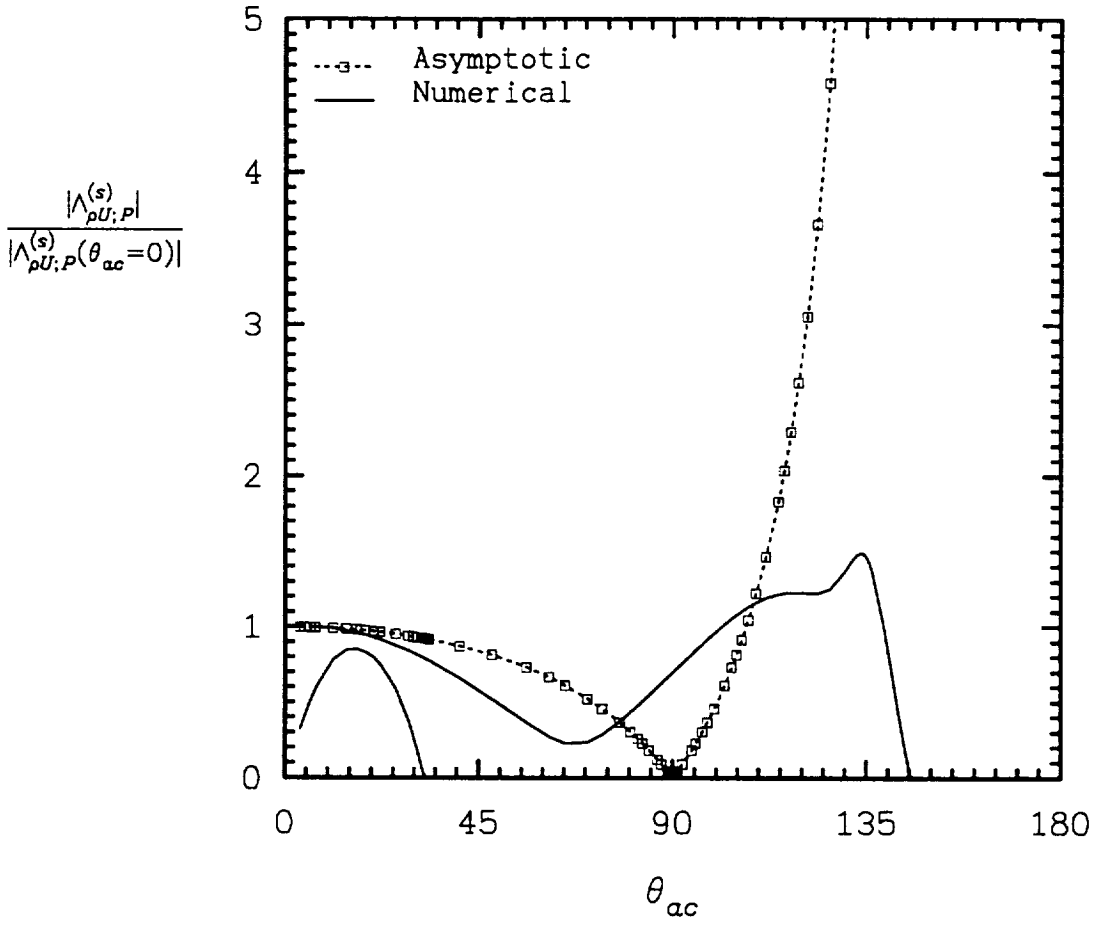


Figure 7(a). Influence of acoustic-wave orientation on  $|\Lambda_{\rho U; P}^{(s)}|$  with  $M = 1.2$ ,  $T_{stgn} = 311$  K,  $R = \sqrt{Re_2} = 955$ ,  $\omega \approx \omega_{1b}$ , and  $\beta_{trs} = 0.0$ .

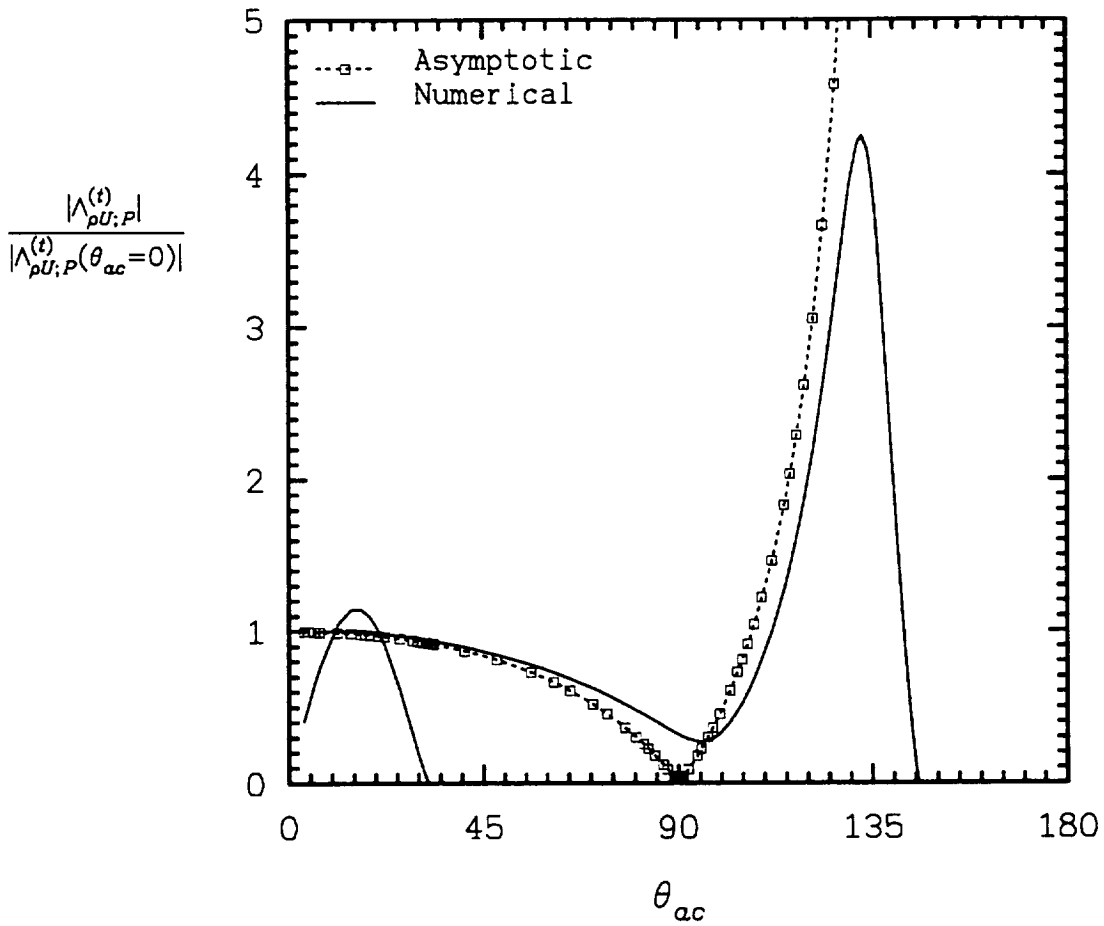


Figure 7(b). Influence of acoustic-wave orientation on  $|\Lambda_{\rho U;P}^{(t)}|$  with  $M = 1.2$ ,  $T_{stgn} = 311$  K,  $R = \sqrt{Re_2} = 955$ ,  $\omega \approx \omega_{1b}$ , and  $\beta_{ins} = 0.0$ .

REPORT DOCUMENTATION PAGE			Form Approved OMB No. 0704-0188	
Public reporting burden for this collection of information is estimated to average 1 hour per response, including the time for reviewing instructions, searching existing data sources, gathering and maintaining the data needed, and completing and reviewing the collection of information. Send comments regarding this burden estimate or any other aspect of this collection of information, including suggestions for reducing this burden, to Washington Headquarters Services, Directorate for Information Operations and Reports, 1215 Jefferson Davis Highway, Suite 1204, Arlington, VA 22202-4302, and to the Office of Management and Budget, Paperwork Reduction Project (0704-0188), Washington, DC 20503.				
1. AGENCY USE ONLY (Leave blank)	2. REPORT DATE June 1994	3. REPORT TYPE AND DATES COVERED Contractor Report		
4. TITLE AND SUBTITLE Acoustic Receptivity of Compressible Boundary Layers: Receptivity via Surface-Temperature Variations		5. FUNDING NUMBERS C NAS1-20059 WU 505-59-50-01		
6. AUTHOR(S) Meelan Choudhari				
7. PERFORMING ORGANIZATION NAME(S) AND ADDRESS(ES) High Technology Corporation Hampton, VA 23666		8. PERFORMING ORGANIZATION REPORT NUMBER		
9. SPONSORING / MONITORING AGENCY NAME(S) AND ADDRESS(ES) National Aeronautics and Space Administration Langley Research Center Hampton, VA 23681		10. SPONSORING / MONITORING AGENCY REPORT NUMBER NASA CR-4599		
11. SUPPLEMENTARY NOTES Langley Technical Monitor: Craig L. Streett				
12a. DISTRIBUTION / AVAILABILITY STATEMENT Unclassified-Unlimited  Subject Category: 34		12b. DISTRIBUTION CODE		
13. ABSTRACT (Maximum 200 words) The Goldstein-Ruban theory has been extended within the quasi-parallel framework of Zaval'skii et al. to study the acoustic receptivity of compressible boundary layers. We consider the receptivity produced in a region of localized, small-amplitude variation in the surface temperature, and compare it with the receptivity that is induced through a similar mechanism by a variation in the suction velocity at the surface. It is found that the orientation of the acoustic wave can have a significant impact on the receptivity process, with the maximum receptivity at a given sound-pressure level being produced by upstream oriented acoustic waves. At sufficiently low Mach numbers, the variation of receptivity with the acoustic-wave orientation can be predicted analytically and is the same for both surface suction and surface heating. However, as a result of the acoustic refraction across the mean boundary layer, the above dependence can become rather complex and, also, dependent on the type of surface nonuniformity. The results also suggest that the receptivity caused by temperature nonuniformities may turn out to be more significant than that produced by the mean-flow perturbations associated with strip suction.				
14. SUBJECT TERMS compressible boundary layers, laminar-turbulent transition, receptivity, acoustics, laminar flow control		15. NUMBER OF PAGES 34		
		16. PRICE CODE A03		
17. SECURITY CLASSIFICATION OF REPORT Unclassified	18. SECURITY CLASSIFICATION OF THIS PAGE Unclassified	19. SECURITY CLASSIFICATION OF ABSTRACT Unclassified	20. LIMITATION OF ABSTRACT Unlimited	